Supporting Information

# Donor−Acceptor−Type Supramolecular Polymers Derived from Robust yet Responsive Heterodimeric Tweezers

*Yu-Kui Tian, Yi-Fei Han, Zhi-Shuai Yang, and Feng Wang**

*CAS Key Laboratory of Soft Matter Chemistry, iChEM (Collaborative Innovation Center of Chemistry for Energy Materials), Department of Polymer Science and Engineering, University of Science and Technology of China, Hefei, Anhui 230026, P. R. China. E-mail: drfwang@ustc.edu.cn.*

## *1. Materials and methods*

Diphenylammonium triflate (DPAT), methylamine, pyrene, copper(I) iodide (CuI), 1,1,3,3-tetramethylguanidine, 4-hydroxybenzaldehyde, 1-pyrenecarboxaldehyde, 1-bromobutane, 4-dimethylamino pyridine (DMAP), 1-pyrenylmethylamine hydrochloride, 1,2-dibromoethane, and *N*-(3-(dimethylamino)propyl)-*N*'-ethylcarbodiimide hydrochloride (EDC•HCl) were reagent grade and used as received. 5-Octadecyloxyisophthalic acid, compound **10** ([Au(C^N^C)(C≡C–$C_6H_5$–OMe–*p*)]), 3-ethynylacetophenone, [Pt(tpy)Cl]($BF_4$), 5-propargyloxyisophthalic acid, and compound **7** were synthesized according to the previously reported procedures).[S1–S6]

$^1$H NMR spectra and two-dimensional diffusion-ordered (DOSY) NMR were collected on a Varian Unity INOVA-300 or INOVA-400 spectrometer with TMS as the internal standard. $^{13}$C NMR spectra were recorded on a Varian Unity INOVA-400 spectrometer at 100 MHz and a Varian Unity INOVA-300 spectrometer at 75 MHz. Electrospray ionization mass spectra (ESI-MS) were obtained on a Bruker Esquire 3000 plus mass spectrometer (Bruker-Franzen Analytik GmbH Breman, Germany) equipped with an ESI interface and ion trap analyzer. Time-of-flight mass spectra (TOF-MS) were obtained on matrix-assisted laser desorption ionization-time of flight (autoflex speed TOF/TOF, Bruker). UV/Vis spectra were recorded on a UV-1800 Shimadzu spectrometer. Viscosity measurements were carried out with Ubbelohde semi-micro dilution viscometer (Shanghai Liangjing Glass Instrument Factory, 0.37 mm inner diameter) at 25 $^o$C in $CHCl_3$. Titration Calorimetry (ITC) experiments were carried out with a Microcal VP-ITC apparatus at 298 K.

For $^1$H NMR dilution experiments, treatment of the chemical shift value (ppm) *vs* the monomer concentration (mol/L) with a non-linear least-squares curve-fitting equation affords the self-association constant. Specifically, the binding constant is calculated according to the Eq. S1:

$$y = P1 + (P2 - P1) \times ((1 + 8 \times x \times P3)^{0.5} - 1)/((1 + 8 \times x \times P3)^{0.5} + 1) \quad \text{(Eq. S1)}$$

P1, P2, and *y* are the chemical shift resonances at uncomplexed state, fully complexed state, and a selected concentration, *x* is the sample concentration. P3 is the self-association constant.

For UV/Vis titration experiments, treatment of the collected absorbance data at 460 nm (*A*) *vs* the concentration of guest added ($C_A$) with a non-linear least-squares curve-fitting equation affords the association constants. Specifically, for 1 : 1 host/guest complexation, binding constants are calculated according to Eq. S2:

$$A = A_0 + \frac{A_{\lim} - A_0}{2C_0}\left[ C_0 + C_A + 1/K_S - \left[ \left( C_0 + C_A + 1/K_S \right)^2 - 4C_0C_A \right]^{1/2} \right] \qquad \text{(Eq. S2)}$$

$A_0$ and $A$ are the absorbance of the host at a selected wavelength with and without presence of the guest, respectively, $[C_0]$ is the total concentration of the host, $[C_A]$ is the concentration of the guest, $A_{lim}$ is the limiting value of absorbance with the presence of excess guest and $K_S$ is the binding constant. The error is a single $K_a$ determination.

## *2. Self-association studies of **1***

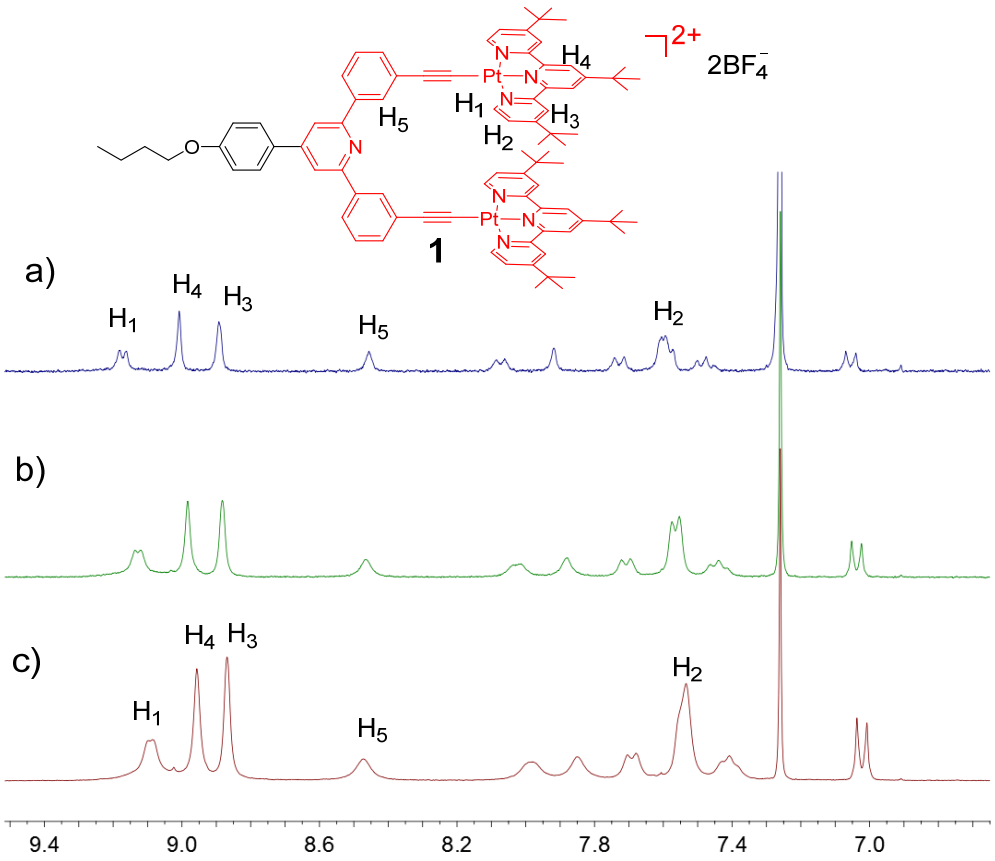


**Figure S1.** $^{1}$H NMR spectra (300 MHz, $CDCl_3$, room temperature) for compound **1** at different concentrations: a) 6.00 mM; b) 3.00 mM; c) 0.60 mM. Only slight chemical shift changes are observed for **1** upon varying its concentrations, suggesting that self-complexation of **1** is negligible due to the presence of bulky *tert*-butyl groups on the pincer units.

## *3. Self-association studies of **3***

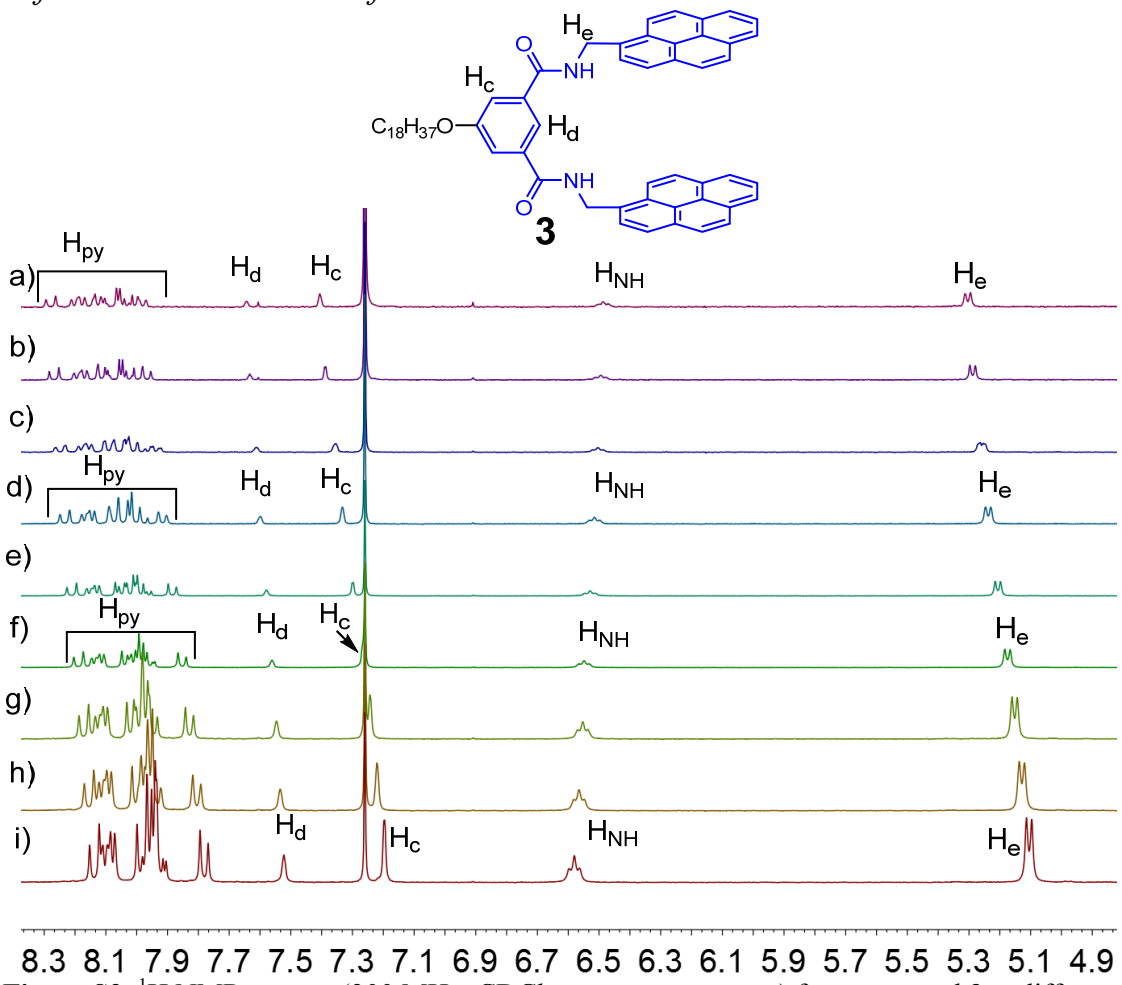


**Figure S2.** $^{1}$H NMR spectra (300 MHz, $CDCl_3$, room temperature) for compound **3** at different concentrations: a) 0.50 mM; b) 1.00 mM; c) 2.00 mM; d) 3.00 mM; e) 4.50 mM; f) 6.00 mM; g) 8.00 mM; h) 10.0 mM; i) 12.0 mM.

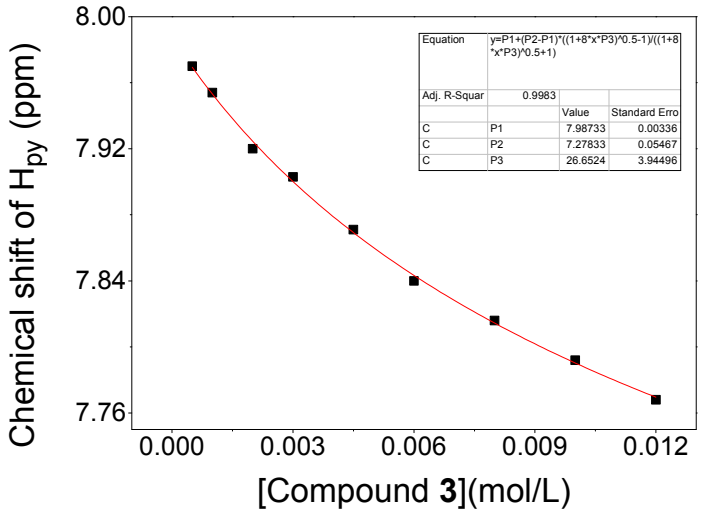

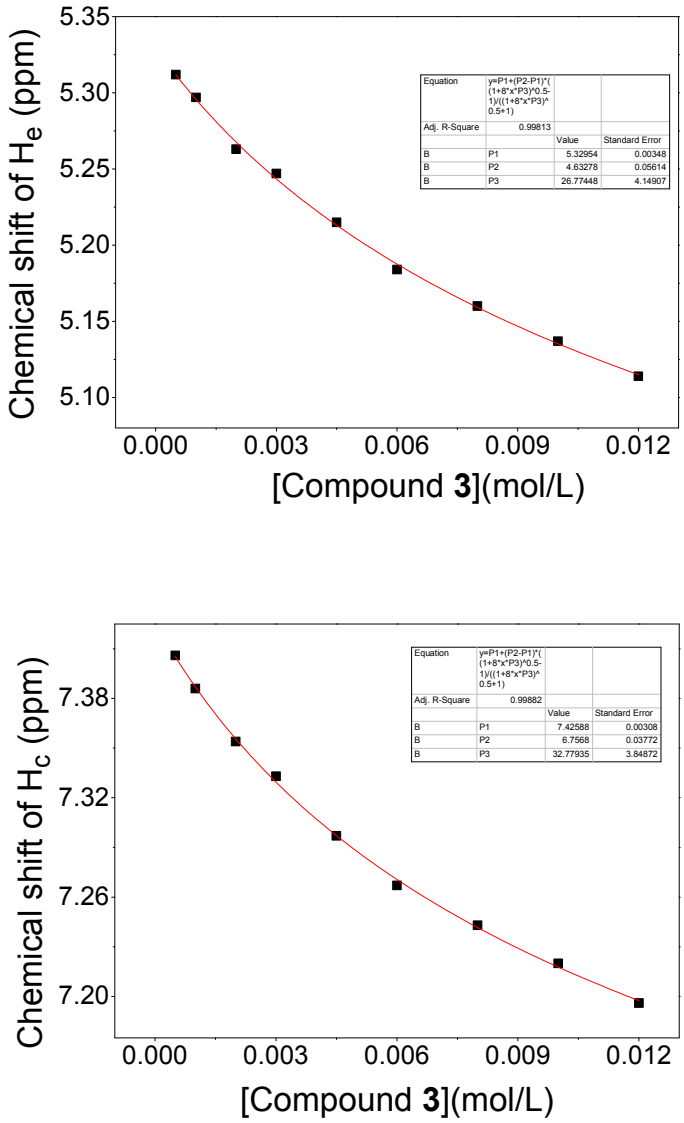


**Figure S3.** Non-linear curve fitting of the protons $H_c$, $H_{py}$, and $H_e$ on 3 *via* $^1$H NMR dilution experiments.[S7] The self-association constant for **3** is determined to be 28.8 ± 4.0 $M^{-1}$, according to the Eq. S1.

## *4. Non-covalent complexation between **1** and **3***

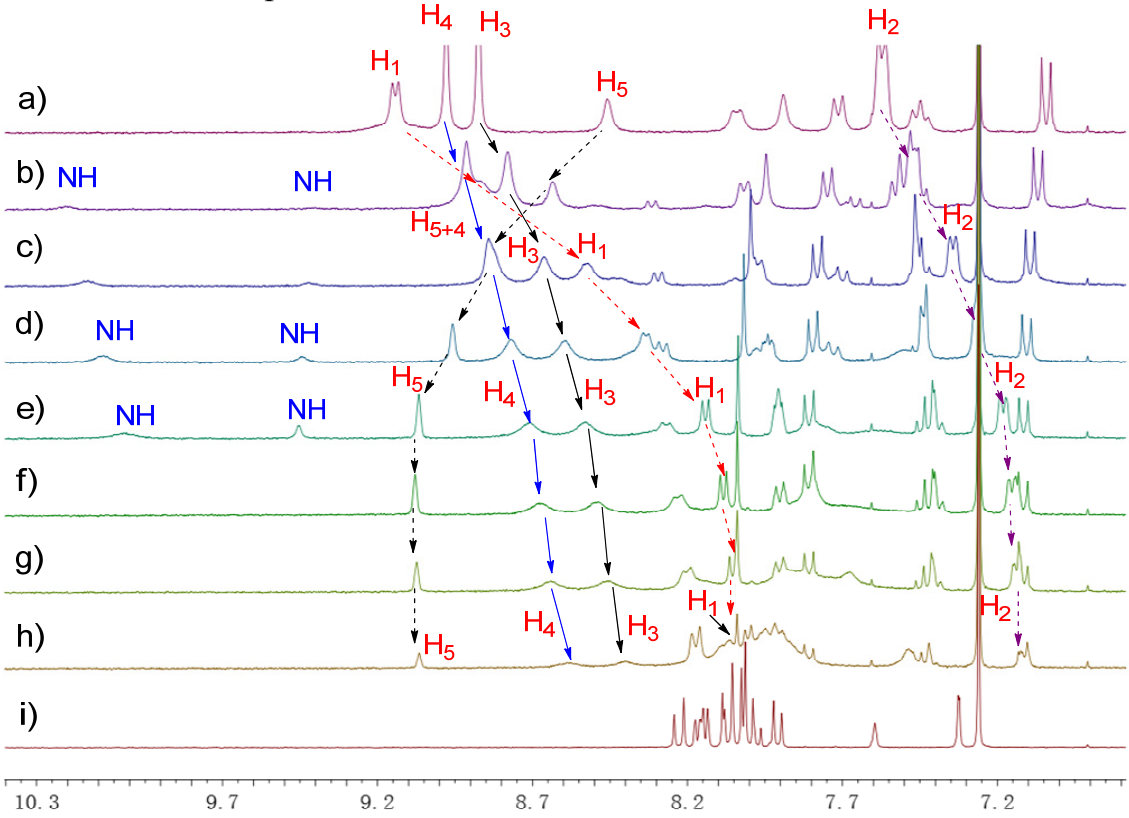


**Figure S4.** $^{1}$H NMR spectra (300 MHz, $CDCl_3$, room temperature) for complex **1**/**3** with different molar ratio: a) 6 : 0; b) 5 : 1; c) 4 : 2; d) 3.5 : 2.5; e) 3 : 3; f) 2.5 : 3.5; g) 2 : 4; h) 1 : 5; i) 0 : 6. $[\mathbf{1}]_0$ and $[\mathbf{2}]_0$ are the initial concentrations of **1** and **3**. $[\mathbf{1}]_0 + [\mathbf{3}]_0 = 4.00$ mM. Upon mixing of the two compounds, protons $H_5$ on **1** show obvious downfield shifts, whereas the terpyridine protons $H_{1\text{-}4}$ on **1** exhibit significant upfield shifts, revealing non-covalent complexation between **1** and **3**. Meanwhile, the two amide protons on **3**, which appear on the significantly downfield position for the complex **1**/**3**, split into two peaks. Such phenomena suggest the different environments for both amides due to the formation of DADA–type heterodimeric tweezering complex.

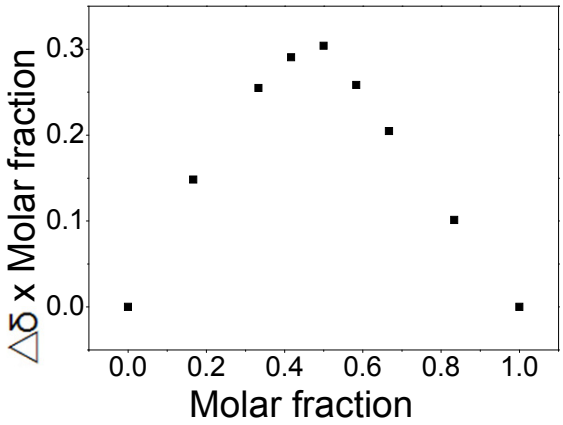


**Figure S5.** Job's plot curve by plotting the chemical shift of $H_5$ against the mole fraction of the guest ($[\mathbf{1}]_0 + [\mathbf{3}]_0 = 4.00$ mM). It shows 1 : 1 binding stoichiometry between **1** and **3**.

## *5. Non-covalent complexation between **1** and 7*

Compound **7**, representing the half-splitting structure for **3**, serves as the model guest and its non-covalent complexation towards **1** is investigated, which facilitates us to interpret the dramatically enhanced binding strength for complex **1**/**3** than that of **1**/**2**.

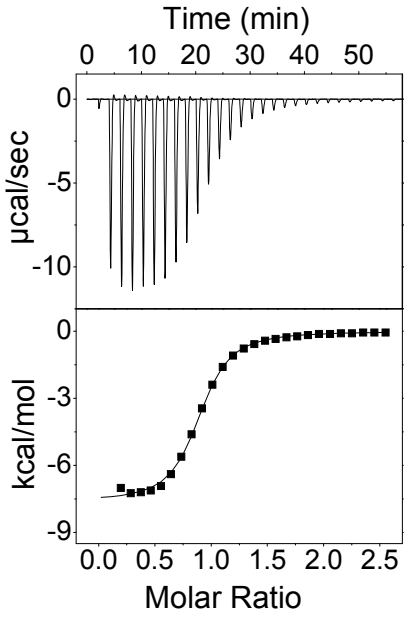


**Figure S6.** Isothermal titration calorimetry experiments by consecutive injecting of **7** (4.00 mM) into the chloroform solution of **1** (0.25 mM). The binding stoichiometry between **1** and **7** is determined to be 1 : 1, as reflected by the abrupt change in the curve. Fitting the exothermic binding isotherm data with the one-site model provides the $K_a$ value of $(1.80 \pm 0.11) \times 10^5\ M^{-1}$ for **1**/**7**.

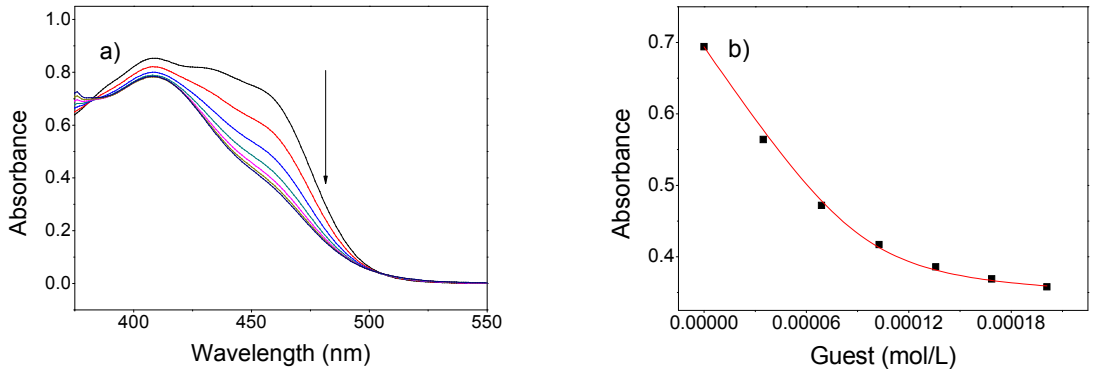


**Figure S7.** a) UV/Vis absorption spectral changes of **1** upon addition of **7**; b) the intensity changes of absorbance at 460 nm upon addition of **7**. The MLCT (metal–to–ligand charge transfer) and LLCT (ligand–to–ligand charge transfer) bands of **1**, predominately locating on the region of approximately 400–500 nm, undergo gradual decrease for the absorption intensity upon progressive addition of **7**. Nonlinear curve-fitting of the collected absorbance data at 460 nm provides the $K_a$ value of $(1.31 \pm 0.35) \times 10^5\ M^{-1}$, which is consistent with the above ITC measurements.

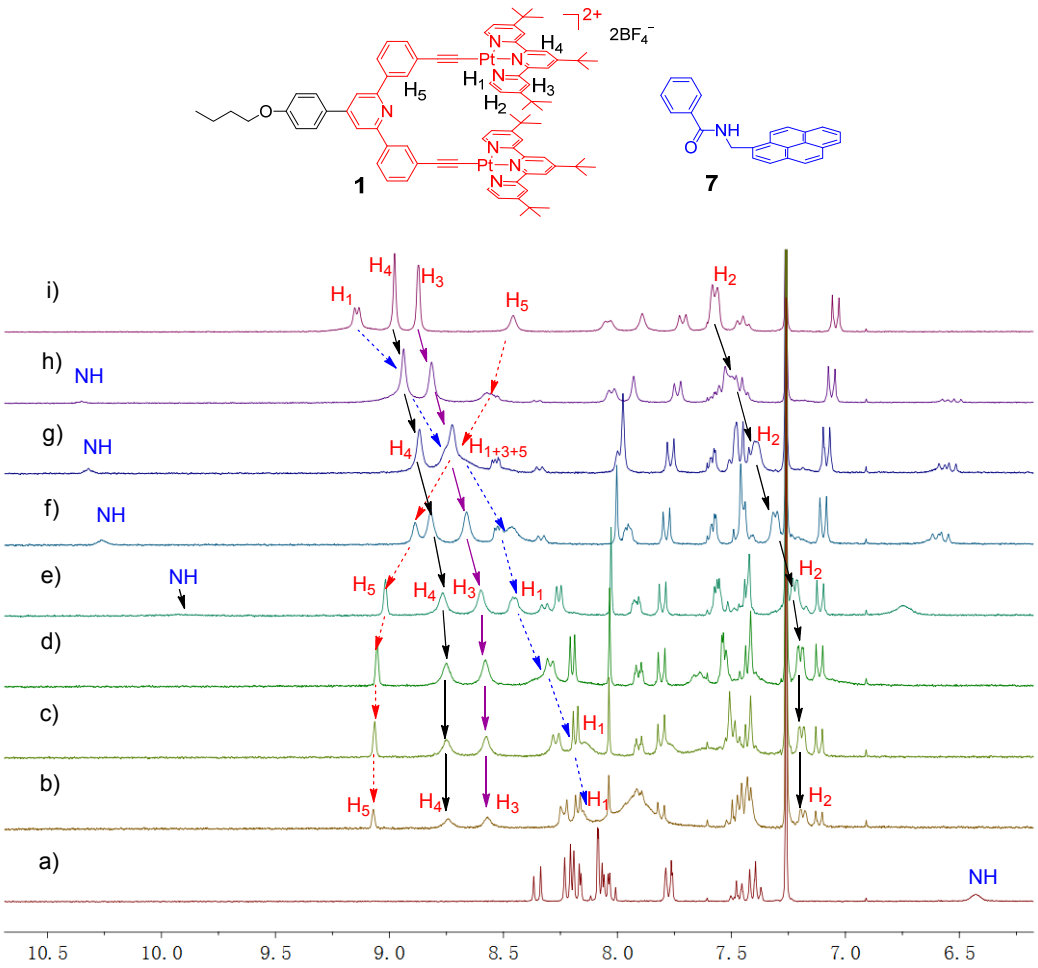


**Figure S8.** $^{1}$H NMR spectra (300 MHz, $CDCl_3$, room temperature) for the complex **1**/**7** with different molar ratio: a) 6 : 0; b) 5 : 1; c) 4 : 2; d) 3.5 : 2.5; e) 3 : 3; f) 2.5 : 3.5; g) 2 : 4; h) 1 : 5; i) 0 : 6. $[\mathbf{1}]_0$ and $[\mathbf{7}]_0$ are the initial concentrations of **1** and **7**. $[\mathbf{1}]_0 + [\mathbf{7}]_0 = 4.00$ mM. Upon mixing of the two compounds, protons $H_5$ on **1** show obvious downfield shifts, whereas the terpyridine protons $H_{1\text{-}4}$ on **1** exhibit significant upfield shifts. Meanwhile, the amide proton on **7** appears on the significantly downfield position for the complex **1**/**7**, revealing the non-covalent complexation between **1** and **7**.

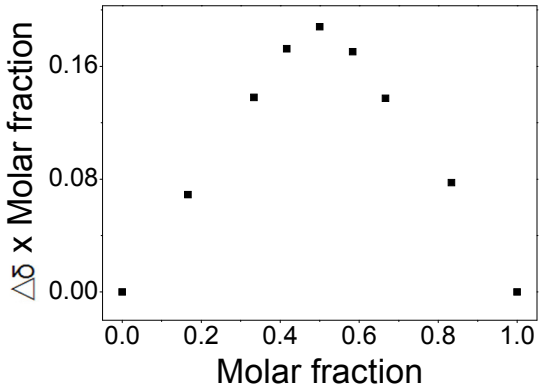


**Figure S9.** Job's plot curve showing 1 : 1 binding stoichiometry between **1** and **7**, by plotting the chemical shift of $H_5$ against the mole fraction of the guest ($[\mathbf{1}]_0 + [\mathbf{3}]_0 = 4.00$ mM). Such phenomenon, which is highly consistent with the above ITC measurement, reveals the non-covalent complexation between **1** and **7** to form ADA–type tweezering complex.

## *6. Non-covalent complexation between **1** and **2***

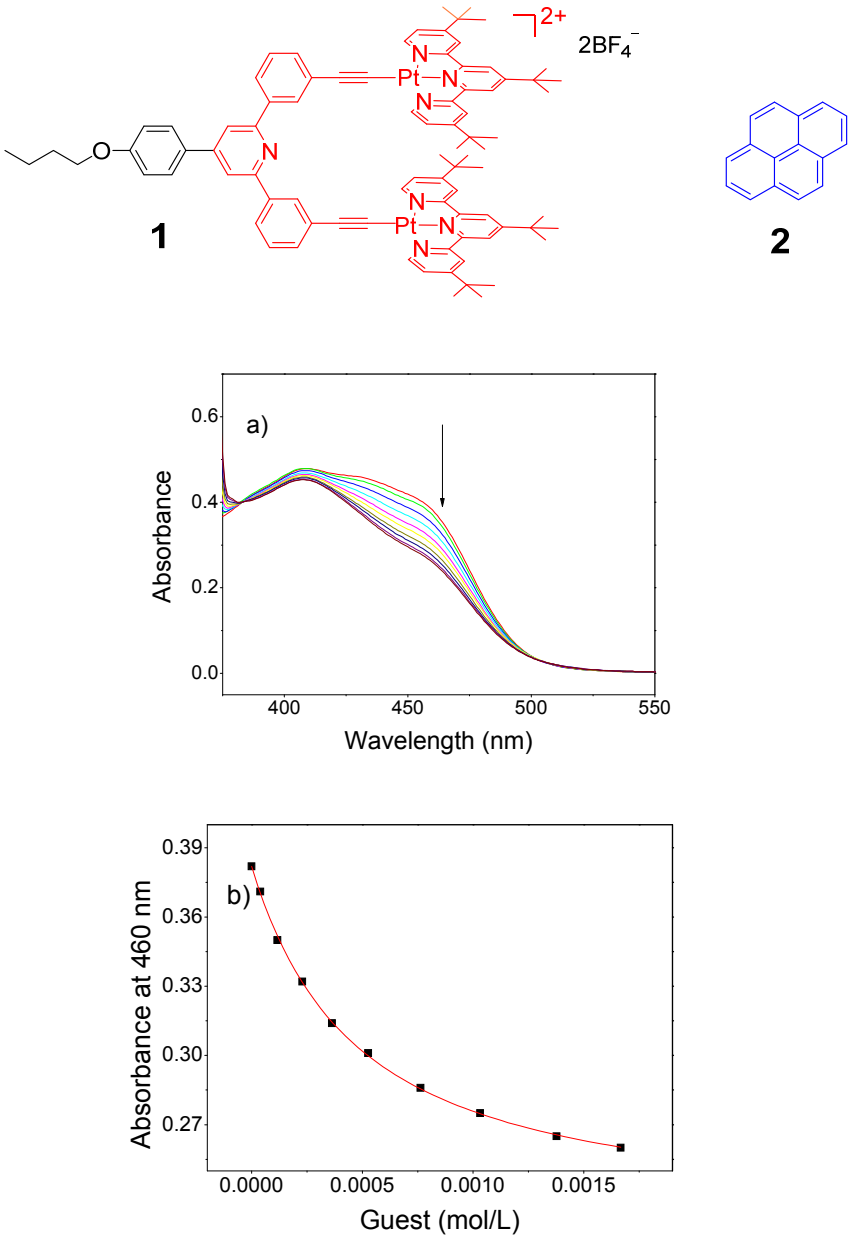


**Figure S10.** a) UV/Vis absorption spectral changes of **1** upon addition of **2**; b) the intensity changes of absorbance at 460 nm upon addition of **2**. The MLCT (metal–to–ligand charge transfer) and LLCT (ligand–to–ligand charge transfer) bands of **1**, predominately locating on the region of approximately 400–500 nm, undergo gradual decrease for the absorption intensity upon progressive addition of pyrene. Nonlinear curve-fitting (red solid line) of the collected absorbance data at 460 nm provides the $K_a$ value of (2.27 ± 0.05) × $10^3$ $M^{-1}$ for **1**/**2**.[S4]

## *7. Non-covalent complexation between **1** and **18***

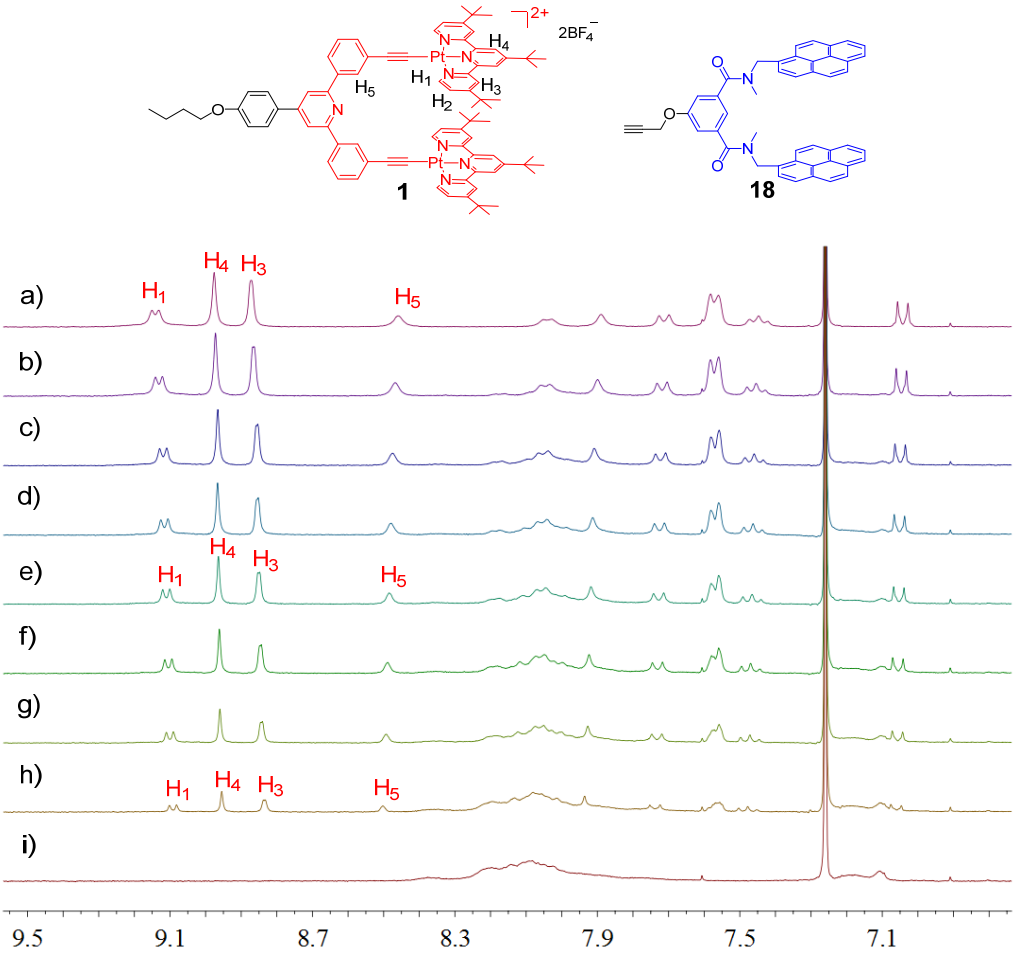


**Figure S11.** $^{1}$H NMR spectra (300 MHz, $CDCl_3$, room temperature) for complex **1**/**18** with different molar ratio: a) 6 : 0; b) 5 : 1; c) 4 : 2; d) 3.5 : 2.5; e) 3 : 3; f) 2.5 : 3.5; g) 2 : 4; h) 1 : 5; i) 0 : 6. $[\mathbf{1}]_0$ and $[\mathbf{18}]_0$ are the initial concentrations of **1** and **18**. $[\mathbf{1}]_0 + [\mathbf{18}]_0 = 4.00$ mM. Upon mixing of the two compounds, slight chemical shift changes occur for the protons on **1**, denoting relatively weak complexation strength between **1** and **18**.

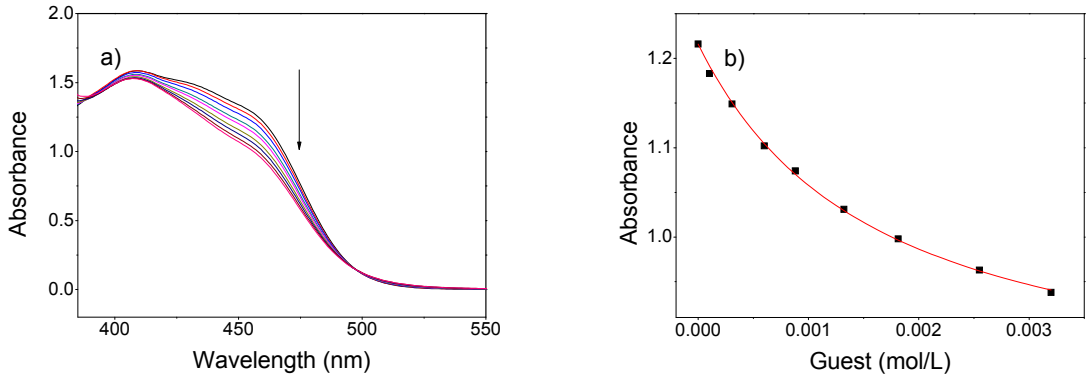


**Figure S12.** a) UV/Vis absorption spectral changes of **1** upon addition of **18**; b) the intensity changes of absorbance at 460 nm upon addition of **18**. Nonlinear curve-fitting of the collected absorbance data at 460 nm provides the $K_a$ value of $(6.67 \pm 0.41) \times 10^2$ $M^{-1}$. The value is considerably thousand times decrease than that of **1**/**3**, suggesting the crucial role of NH–N and NH–π interactions to maintain strong binding affinity for **1**/**3**.

## *8. Addition of HFIP into the chloroform solutions of **1/3** and **1/10***

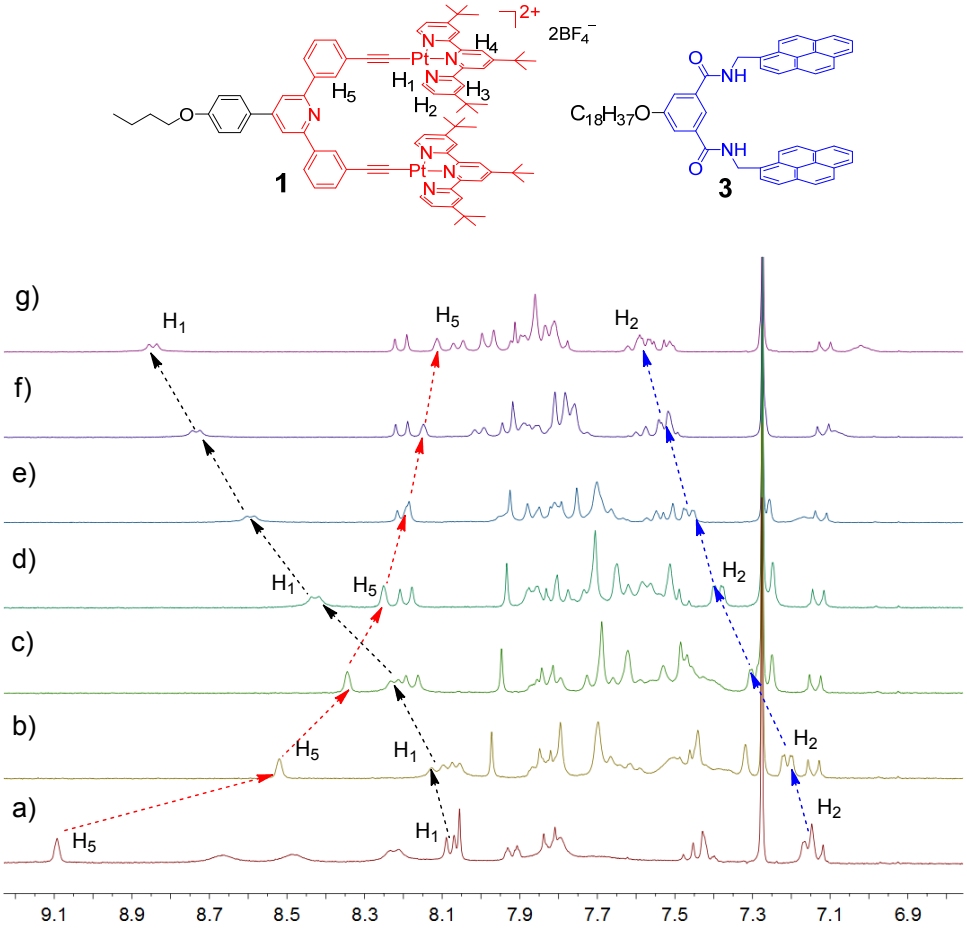


**Figure S13.** $^{1}$H NMR spectra (300 MHz, $CDCl_3$, room temperature) of an equimolar solution of **1** and **3** ([**1**] = [**3**] = 3.00 mM) with different percentage of HFIP (*v*/*v*): a) 0%; b) 1.6%; c) 3.2%; d) 4.8%; e) 6.3%; f) 7.7%; g) 9.1%. Upon gradual addition of HFIP, proton $H_5$ on **1** undergoes significant upfield shift, whilst noticeable downfield shifts are observed for $H_{1\text{-}2}$. The chemical shift changes for all of these protons are contrary to those of the non-covalent complexation process, denoting the weakening of binding strength for **1**/**3** triggered by HFIP.

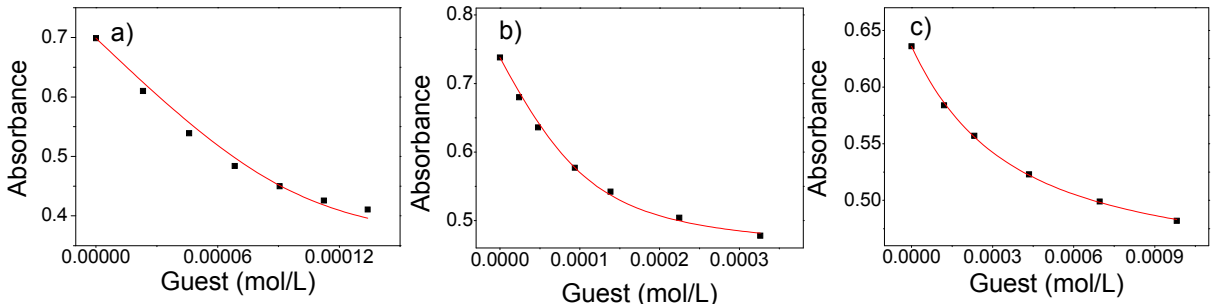


**Figure S14.** The intensity changes of absorbance at 460 nm for **1** ($1.00 \times 10^{-4}$ M) upon stepwise addition of **3** with different solvent compositions: a) 2% (*v*/*v*) HFIP in $CHCl_3$, $K_a = (1.00 \pm 0.67) \times 10^5$ $M^{-1}$; b) 4% (*v*/*v*) HFIP in $CHCl_3$, $K_a = (3.33 \pm 0.59) \times 10^4$ $M^{-1}$; c) 8% (*v*/*v*) HFIP in $CHCl_3$, $K_a = (3.33 \pm 0.21) \times 10^3$ $M^{-1}$. Such results indicate that 8% HFIP results in surprisingly thousand times decrease for the binding affinity between **1** and **3**.

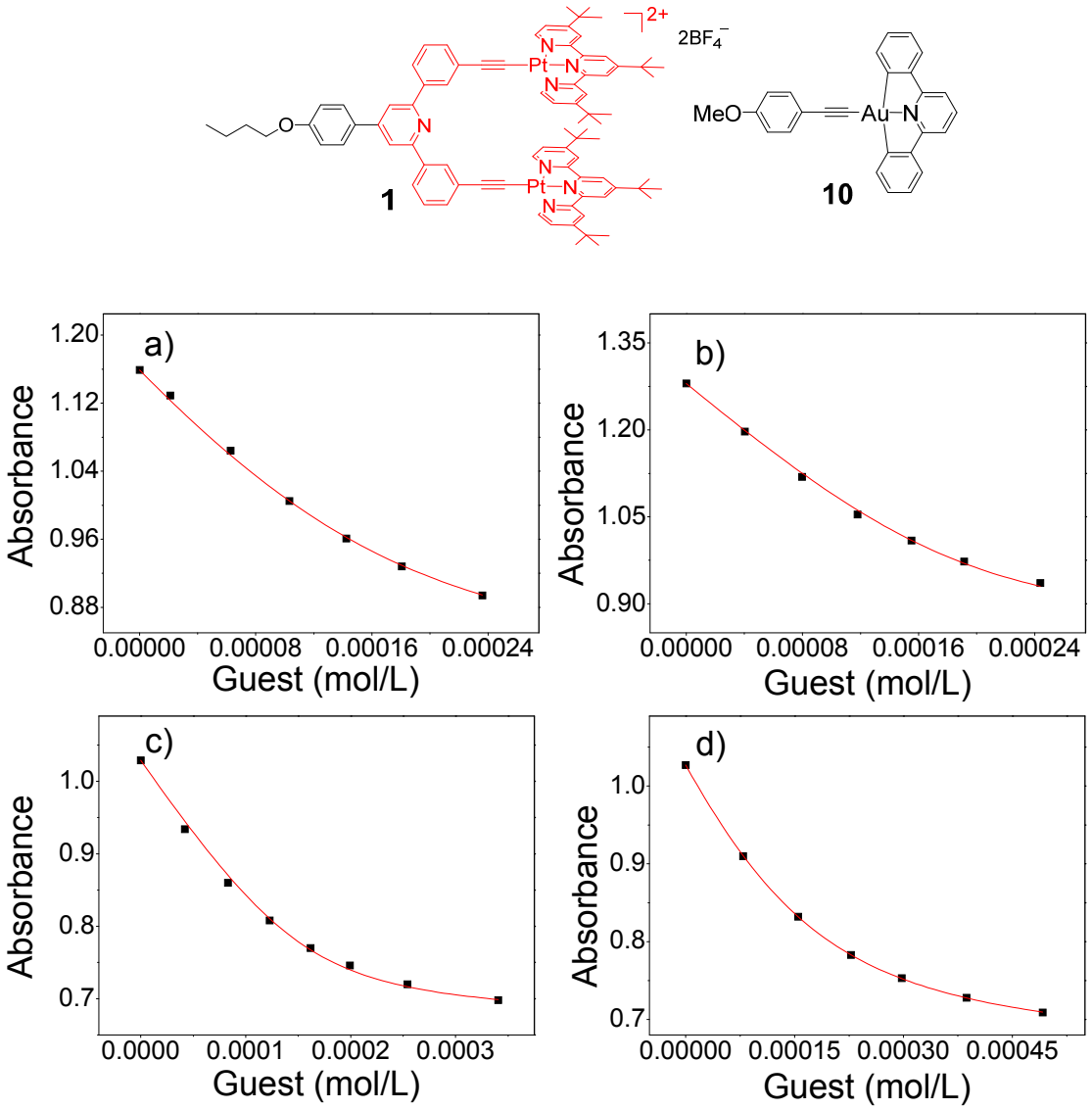


**Figure S15.** The intensity changes of absorbance at 460 nm for **1** ($1.00 \times 10^{-4}$ M) upon stepwise addition of **10** at different solvent compositions: a) 0% (*v*/*v*) HFIP in $CHCl_3$, $K_a = (2.00 \pm 0.57) \times 10^4$ $M^{-1}$; b) 2% (*v*/*v*) HFIP in $CHCl_3$, $K_a = (5.00 \pm 2.50) \times 10^4$ $M^{-1}$; c) 4% (*v*/*v*) HFIP in $CHCl_3$, $K_a = (5.00 \pm 1.10) \times 10^4$ $M^{-1}$; d) 8% (*v*/*v*) HFIP in $CHCl_3$, $K_a = (1.43 \pm 0.02) \times 10^4$ $M^{-1}$. The binding strength for **1**/**10**, which is solely driven by donor–acceptor interactions without the participation of hydrogen bonds, is slightly influenced by HFIP. Hence, it is evident that HFIP-triggered weakening of binding strength for **1**/**3** and **1**/**7** mainly stems from the breakage of intermolecular hydrogen bonds, whereas solvent polarity effects brought by HFIP could be excluded to a large extent.

## *9. Protonation/deprotonation of **1** via successive addition of TFA and TEA*

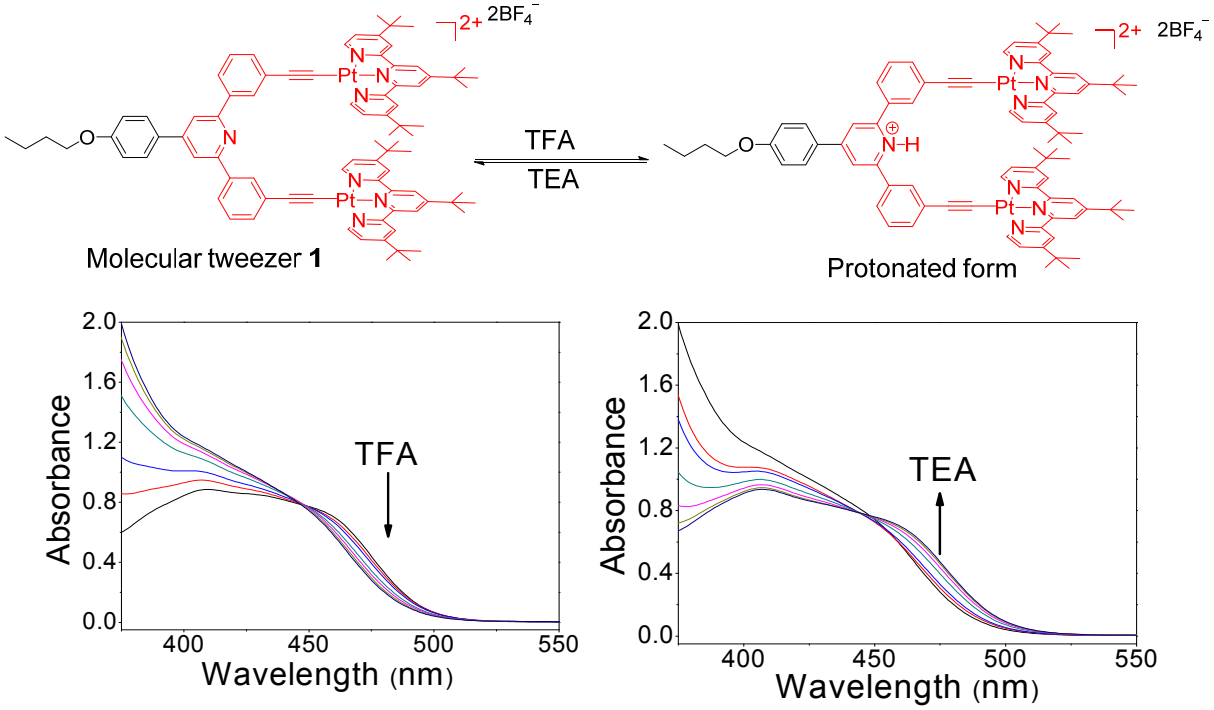


**Figure S16.** Protonation/deprotonation of **1** *via* successive addition of TFA and TEA. Upon addition of TFA (*left*), the intensity for the low-energy LLCT band locating around 450–500 nm progressively decreases, whereas the relatively higher-energy absorption band gradually strengthens, accompanying with the appearance of a clear isobestic point at 447 nm. Blue-shifting of the LLCT band is attributed to the decreased electron-donating ability for the diphenylpyridine alkynyl ancillary ligand, thus reflecting the efficient conversion of **1** to its protonated form. The reversal transition is further validated by the addition of triethylamine (*right*), leading to the restore of the original UV-Vis absorption bands of **1**.

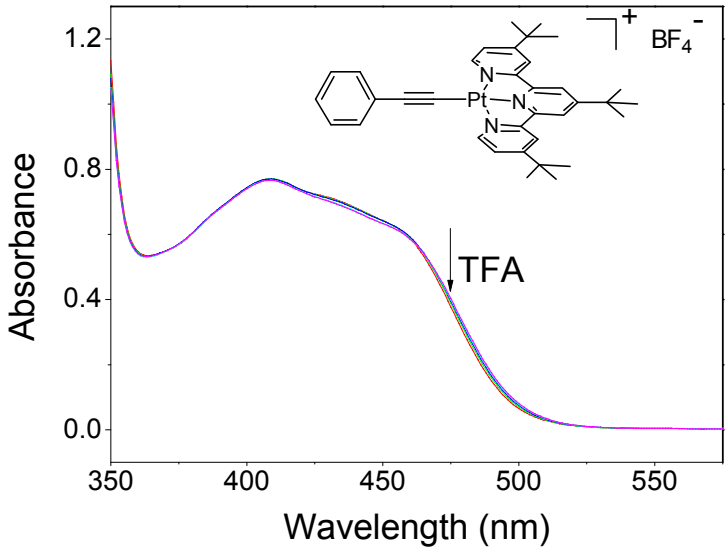


**Figure S17.** UV/Vis absorption spectral changes of Pt (N^N^N) upon addition of TFA. No obvious changes occur for the UV/Vis absorption peaks of Pt (N^N^N), suggesting that the bis[alkynylplatinum(II)] terpyridine units on **1** could not be directly protonated by TFA.

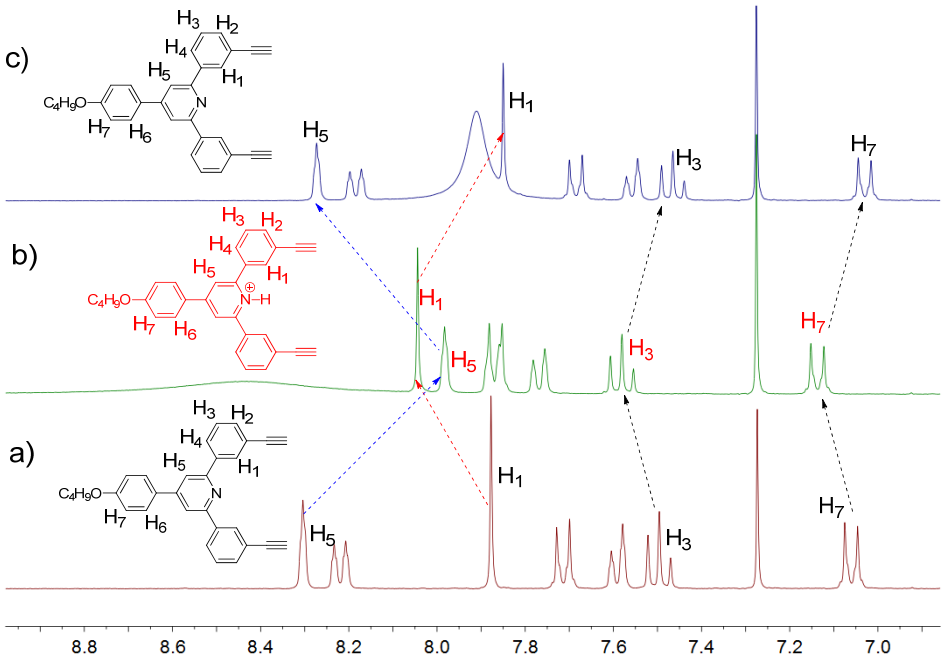


**Figure S18.** $^{1}$H NMR spectra (300 MHz, chloroform-*d*, room temperature) of **12** (3.00 mM) upon stepwise addition of TFA and TEA: a) 0 μL of TFA; b) 10 μL of TFA; c) 10 μL of TFA and 25μL of TEA. Upon addition of TFA to the chloroform solution of **12**, protons $H_{1, 3, 7}$ exhibit obvious downfield shifts. Meanwhile, proton $H_5$ shows dramatic upfield shifts. Further addition of TEA leads to the restore of the original structure. Such results definitely support that TFA imparts positive charges exactly on the pyridine unit of **1**.

## *10. TFA-triggered weakening of binding strength for **1/3***

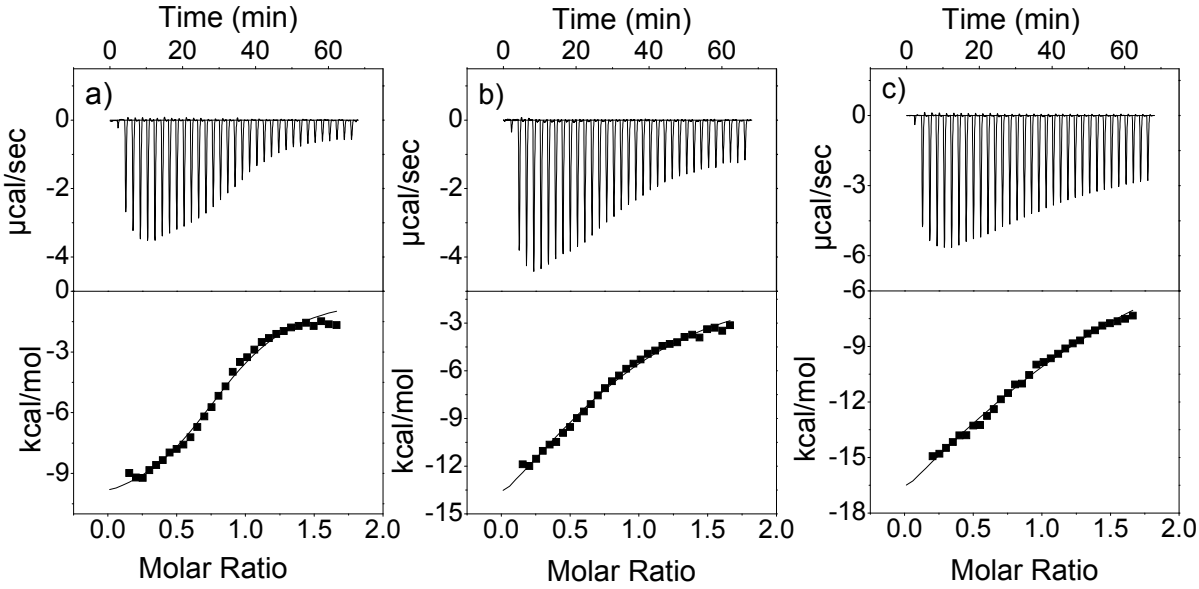


**Figure S19.** ITC data for the titration of **3** ($1.00 \times 10^{-3}$ M) into the solution of **1** ($1.00 \times 10^{-4}$ M) at different solvent compositions: a) 0.021% (*v*/*v*) TFA in $CHCl_3$, $K_a = (8.14 \pm 0.88) \times 10^4$ $M^{-1}$; b) 0.083% (*v*/*v*) TFA in $CHCl_3$, $K_a = (1.71 \pm 0.20) \times 10^4$ $M^{-1}$; c) 0.17% (*v*/*v*) TFA in $CHCl_3$, $K_a = (6.40 \pm 1.30) \times 10^3$ $M^{-1}$. It is evident that 0.17% (*v*/*v*) TFA brings about 350 times decrease for the complexation strength between **1** and **3**.

## *11. DOSY measurements for oligomers **9***

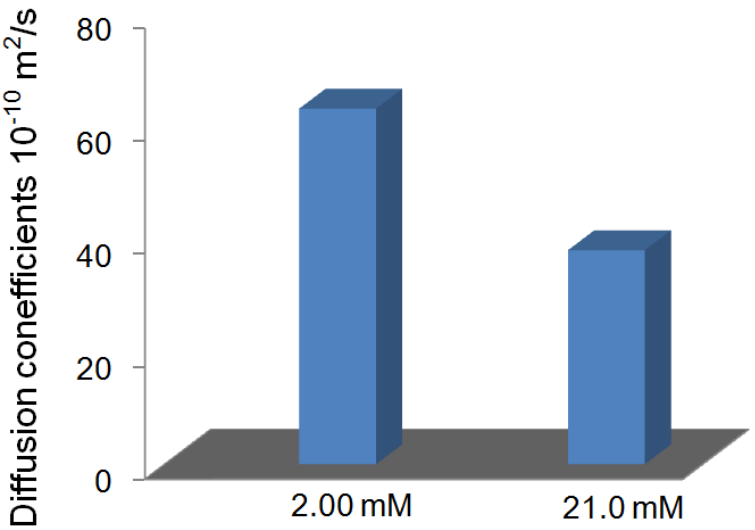


**Figure S20.** The diffusion coefficients of supramolecular oligomers **9** (derived from equimolar mixing of **4** and **8**) at different monomer concentrations. As the concentration of **4** increases from 2.00 mM to 21.0 mM, the measured diffusion coefficients vary from $6.31 \times 10^{-9}$ $m^2$ $s^{-1}$ to $3.80 \times 10^{-9}$ $m^2$ $s^{-1}$, which only exhibits 1.7 times change. When comparing the size variations of **6** and **9**, it is evident that the enhanced binding affinity for the non-covalent repeating units is beneficial for the fabrication of supramolecular polymeric assemblies with larger size.

*12. Specific viscosity measurements for supramolecular polymers **6** and oligomers **9***

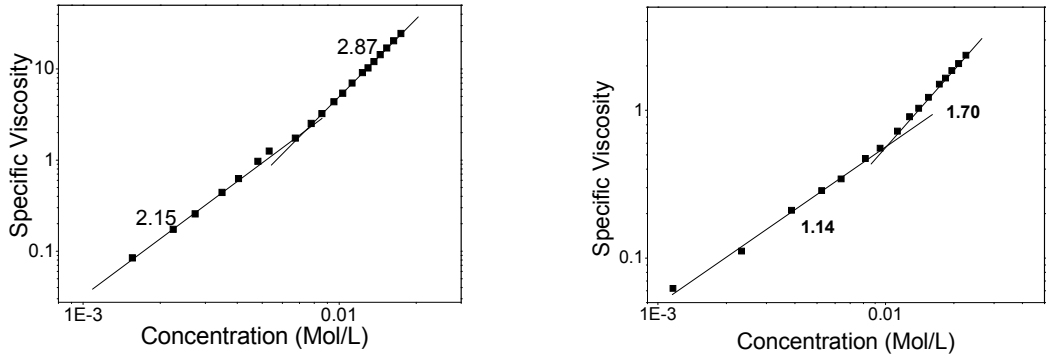


**Figure S21.** The double logarithmic plot of specific viscosity of **6** (*left*) and **9** (*right*) *versus* the monomer concentration (chloroform, 298 K). For both assemblies, they show distinct slope changes, accompanying with the critical points, which reveal ring-chain transitions from cyclic oligomers to supramolecular polymers at high monomer concentrations. Notably, above the critical polymerization concentration, the slope value (2.87) of **6** is significantly higher than that of **9** (slope = 1.70), revealing the enhanced supramolecular polymerization for **6** at high monomer concentrations.

## *13. Theoretical calculations for the optimized geometries of complexes **1/2**, **1/3**, **1/7** and **1/18***

As we know, X-ray crystallography is a powerful technique to elucidate the non-covalent complexation structures. For both complexes **1**/**3** and **1**/**7**, although many attempts have been made, we still failed to grow large, high quality single crystals suitable for X-ray crystallography measurements. As an alternative way, we tuned to rely on the theoretical calculations to get deeper insights into the structural information for these two complexes.

With the utilization of Gaussian 09 software,[S8] a convenient approach is to perform the calculation of complexes **1/3** and **1/7** on the basis of the single crystal structure of **1** (see Figure S22a), since the single crystal reflects the most feasible conformation for the specific compound. Although the single crystal for **1** has not been obtained by us, we fortunately found that Yam *et al.* (*Chem. Sci.* **2012**, *3*, 1185−1191) have already reported a single crystal structure for another molecular tweezer, which is almost identical to **1** in our system. Hence, such a crystal structure serves as a model to simulate the structure of **1**, and thereby it is capable to carry out the optimization for complexes **1/3** and **1/7** *via* the freezing of atomic coordinate for **1**. Unexpectedly, by means of ONIOM model with semi-empirical PM6 and DFT/B3LYP/6-31G(d) as basis sets,[S9-S10] the geometries for both complexes **1/7** and **1/3** could be successfully obtained with reasonable cost (see Figure S22b and S22c). It is worthy of note that, for both complexes **1/7** and **1/3** in the optimized geometries, they could not only exhibit hydrogen bonding interactions, but also demonstrate electron donor–acceptor interaction between alkynylplatinum (II) terpyridine and pyrene moieties (see Table S1), which is more consistent with the $^{1}$H NMR and UV-Vis experimental results. Moreover, structural optimization was also performed for complexes **1/2** and **1/18** (see Figure S22d and S22e), which are based on the ONIOM model calculations. For the optimized structure of **1**/**2**, pyrene shows partial overlapping with the alkynylplatinum (II) terpyridine pincer, and the distance for the pyrene donor and alkynylplatinum (II) terpyridine acceptor is around 3.54 Å. Notably, for the optimized geometry of complex **1/18**, rather weak π-surface overlapping exists between the donor and acceptor units. In detail, the D–A distance within the cavity is approximately 4.50 Å, whilst the pyrene lying on the outer face of **1** doesn't show any effective overlapping with the alkynylplatinum (II) terpyridine pincer (see Figure S22e). Such results are highly consistent with titration experiments, for which the binding affinity for complex **1/3** ($K_a$ = (2.23 ± 0.28) × $10^6$ $M^{-1}$) is significantly higher than that of the counterpart complex **1/18** ($K_a$ = (6.67 ± 0.71) × $10^2$ $M^{-1}$).

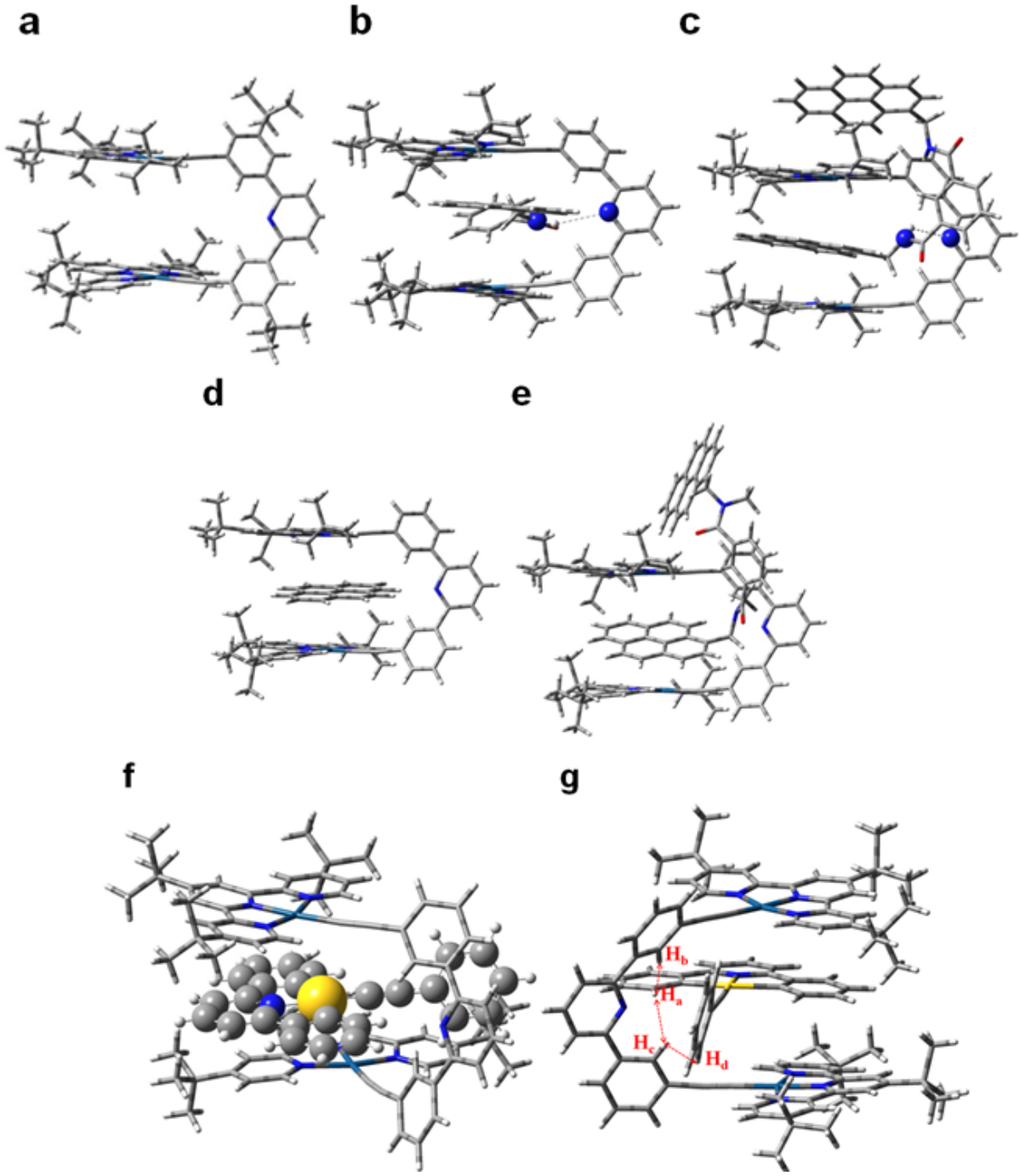


**Figure S22.** (*a*) The single crystalline structure of molecule tweezer reported by Yam. Optimized structure for (*b*) complex **1**/**7**, (*c*) complex **1**/**3**, (*d*) complex **1**/**2**, (*e*) complex **1**/**18** and (*f*) complex **1**/**10** with frozen atoms *via* ONIOM model. During the optimization processes, all atoms in **1** were frozen and calculated under semi-empirical PM6. The guests involved in the non-covalent complexes are optimized under DFT/B3LYP/6-31G(d). Dash lines refer to NH–N hydrogen bond. Guest **10** was optimized under DFT/PBEPBE/6-31G+(d) combined with SDD (Stuttgart) core potentials. (g) The red double arrows dash lines represent the possible NOE phenomenon between $H_a$/$H_b$, $H_a$/$H_c$ and $H_c$/$H_d$, respectively.

**Table S1.** Parameters for hydrogen bonding and donor-acceptor (D-A) interactions in the optimized structures of **1**/**3**, **1**/**7**, **1**/**2** and **1**/**18**

| Complex | **1**/**3** | **1**/**7** | **1**/**2** | **1**/**18** |
|---|---|---|---|---|
| **Parameters for hydrogen bonds** | | | | |
| NH–N length | 3.08 Å | 2.94 Å | none | none |
| NH–N angle | 128.4˚ | 152.1˚ | none | none |
| **Parameters for D-A interactions** | | | | |
| D-A distance[1] in cavity | 3.30 Å | 3.48 Å | 3.54 Å | 4.50 Å |
| | 3.80 Å | none | none | none |
| D-A distance out of cavity | 4.09 Å | none | none | none |
| $K_a$ ($M^{-1}$) | $2.23\times10^6$ | $1.80\times10^5$ | $2.27\times10^3$ | $6.67\times10^2$ |

Note: [1] D-A distance refers to the distance between the alkynylplatinum terpyridine planes and the centroid atom of pyrene, considering that the donor and acceptor moties are not strictly parallel with each other.

## *14. Synthetic routes to the targeted compounds **1** and **3***

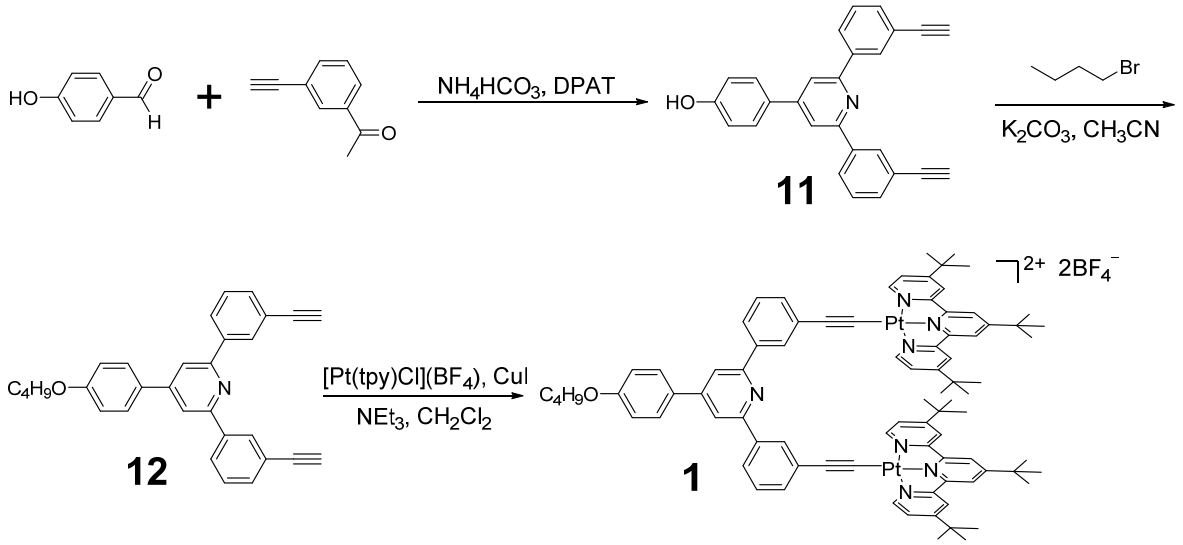


**Figure S23.** Synthetic routes to compound **1**.

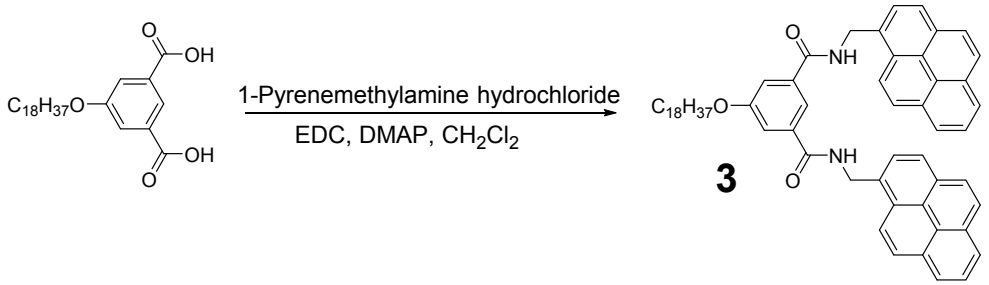


**Figure S24.** Synthetic routes to compound **3**.

## *14.1 Synthesis of compound **12***

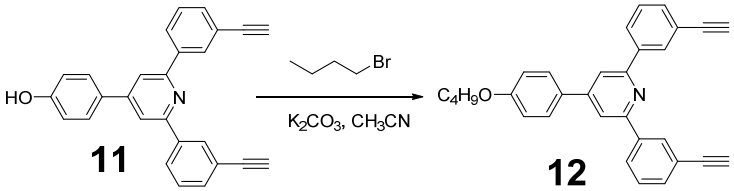


1-Bromobutane (2.74 g, 20.0 mmol), **11** (2.00 g, 5.39 mmol), and $K_2CO_3$ (6.00 g, 43.5 mmol) in $CH_3CN$ (100 mL) were stirred at 90 $^oC$ for 36 hours. After the reaction was complete, the solvent was evaporated under reduced pressure and the residue was extracted with $H_2O/CH_2Cl_2$. The combined organic extracts were dried over anhydrous $Na_2SO_4$ and evaporated with a rotary evaporator, and the residue was purified by flash column chromatography (petroleum ether/$CH_2Cl_2$, 10 : 1 *v*/*v* as the eluent) to afford **12** as a white solid (1.89 g, 82%). Mp: 98.3−99.9 $^oC$. $^1H$ NMR (300 MHz, $CDCl_3$, room temperature) $\delta$ (ppm): 8.29 (s, 2H), 8.21 (d, $J$ = 8 Hz, 2H), 7.86 (s, 2H), 7.74–7.65 (m, 2H), 7.58 (d, $J$ = 8 Hz, 2H), 7.48 (t, $J$ = 8 Hz, 2H), 7.05 (d, $J$ = 9 Hz, 2H), 4.05 (t, $J$ = 7 Hz, 2H), 3.15 (s, 2H), 1.89–1.76 (m, 2H), 1.56 (m, 2H), 1.01 (t, $J$ = 7 Hz, 3H). $^{13}C$ NMR (75 MHz, $CDCl_3$, room temperature) $\delta$ (ppm):160.2, 156.5, 150.0, 139.8, 132.6, 130.7, 130.6, 128.8, 128.3, 127.7,

122.5, 116.9, 115.1, 83.7, 67.9, 53.4, 31.3, 19.3, 13.9. ESI–MS *m/z*: calcd for $[M + H]^+$, $C_{31}H_{26}NO$, 428.2014; found, 428.2010.

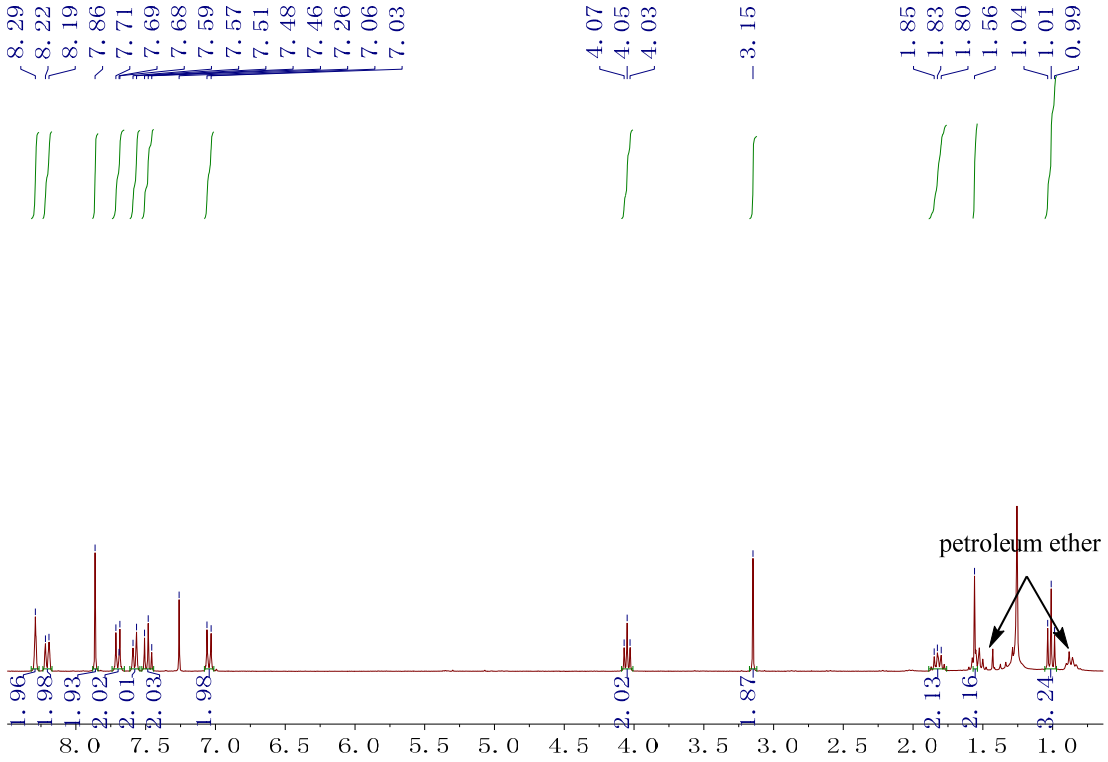


**Figure S25.** $^1$H NMR spectrum (300 MHz, $CDCl_3$, room temperature) of compound **12**.

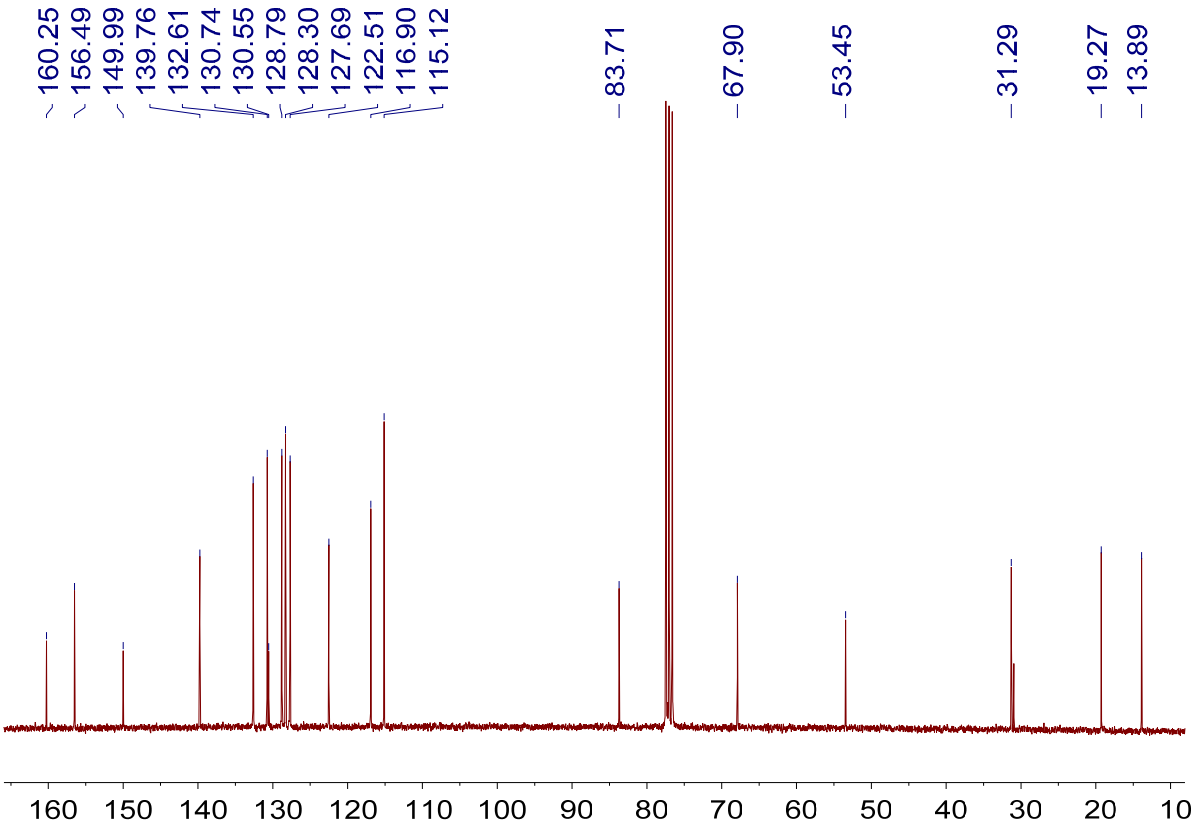


**Figure S26.** $^{13}$C NMR spectrum (75 MHz, $CDCl_3$, room temperature) of compound **12**.

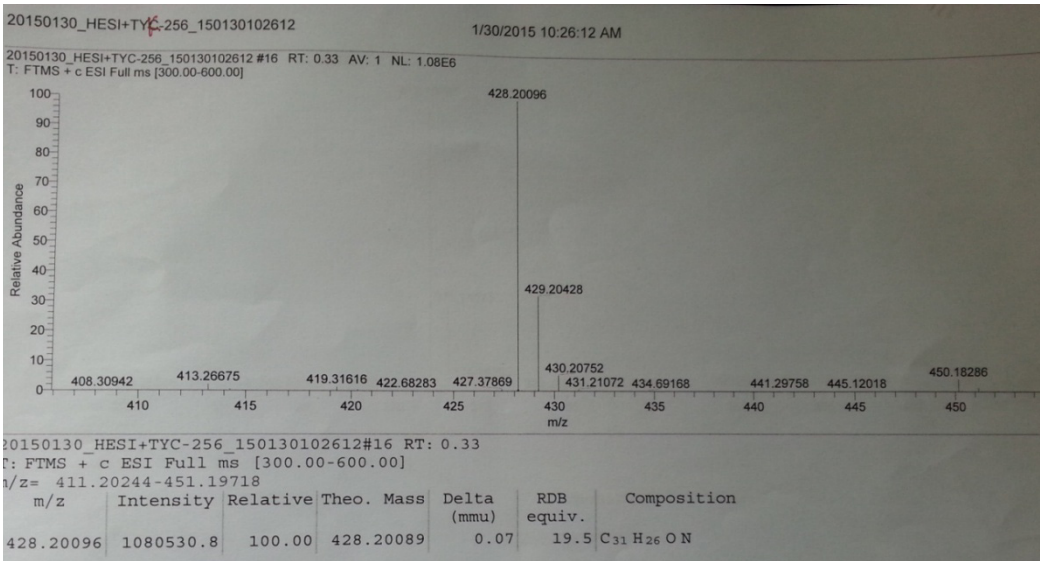


**Figure S27.** Electrospray ionization spectrum of compound **12**.

## *14.2 Synthesis of compound **1***

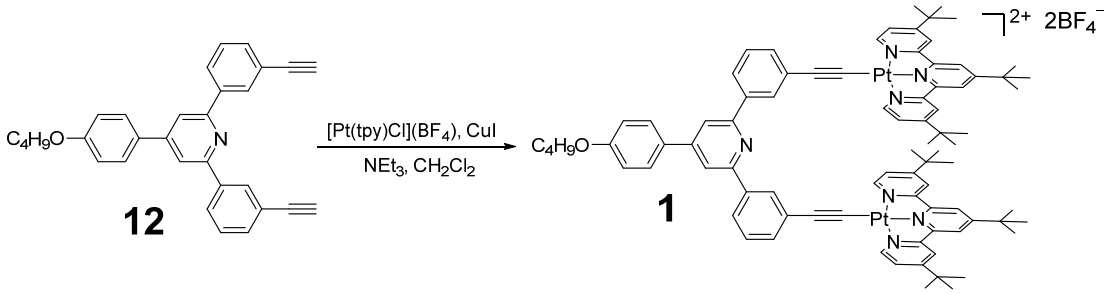


Compound **12** (600 mg, 1.40 mmol), [Pt(tpy)Cl](BF$_4$) (2.15 g, 3.00 mmol), CuI (50 mg, 0.25 mmol) and NEt$_3$ (20 mL) in 200 mL of $CH_2Cl_2$ were stirred at room temperature for 48 hours under nitrogen atmosphere. The mixture was evaporated under reduced pressure and the residue was purified by column chromatography (alumina, $CH_3OH/CH_2Cl_2$, 100 : 1 *v*/*v* as the eluent) to afford **1** as an orange solid (1.58 g, 63%). The compound **1** began to decompose before reaching the melting point. $^1$H NMR (300 MHz, $CDCl_3$, room temperature) $\delta$ (ppm): 9.15 (d, $J$ = 6 Hz, 4H), 8.98 (s, 4H), 8.88 (s, 4H), 8.46 (s, 2H), 8.04 (m, 2H), 7.90 (s, 2H), 7.72 (d, $J$ = 9 Hz, 2H), 7.58 (m, $J$ = 6 Hz, 6H), 7.45 (t, $J$ = 8 Hz, 2H), 7.05 (d, $J$ = 9 Hz, 2H), 4.05 (t, $J$ = 7 Hz, 2H), 1.88–1.75 (m, 2H), 1.65 (m, 20H), 1.53 (m, 36H), 1.00 (t, $J$ = 7 Hz, 3H). $^{13}$C NMR (100 MHz, $CDCl_3$, room temperature) $\delta$ (ppm): 168.9, 167.4, 160.3, 158.8, 156.6, 153.8, 149.3, 139.4, 132.4, 130.7, 128.5, 128.1, 127.2, 125.0, 124.2, 122.5, 115.2, 104.3, 98.5, 68.0, 53.4, 37.8, 36.6, 31.3, 30.8, 30.4, 19.3, 13.9. ESI–MS *m*/*z*: calcd for $[M - 2BF_4]^{2+}$, $C_{85}H_{93}N_7OPt_2$, 808.3354; found, 808.3387.

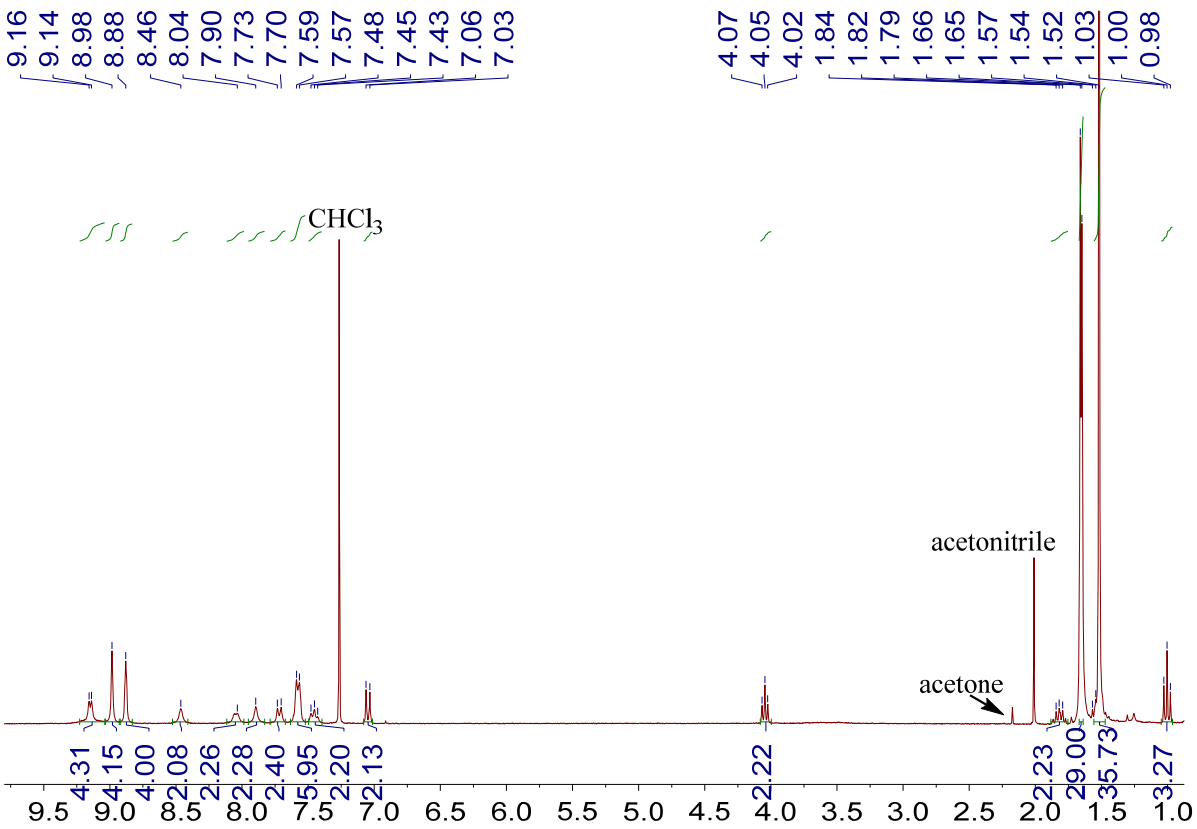


**Figure S28.** $^{1}$H NMR spectrum (300 MHz, $CDCl_3$, room temperature) of compound **1**.

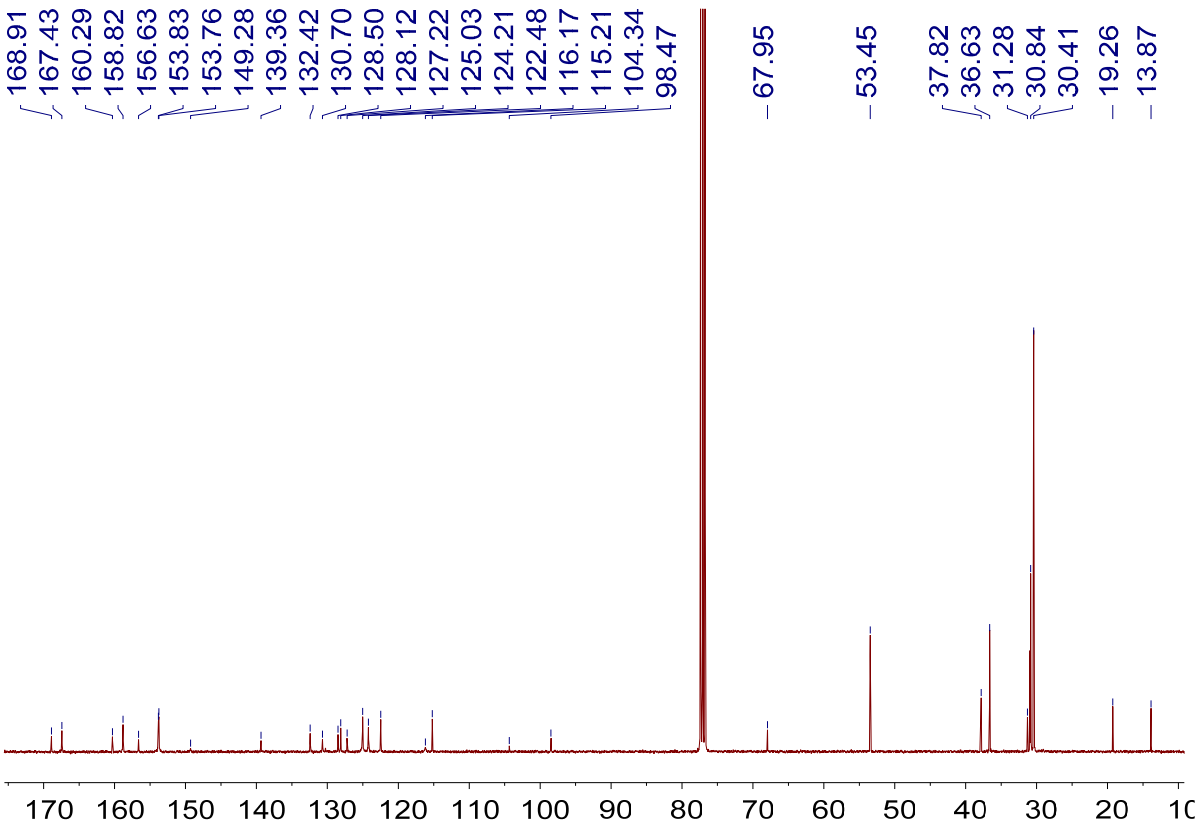


**Figure S29.** $^{13}$C NMR spectrum (75 MHz, $CDCl_3$, room temperature) of compound **1**.

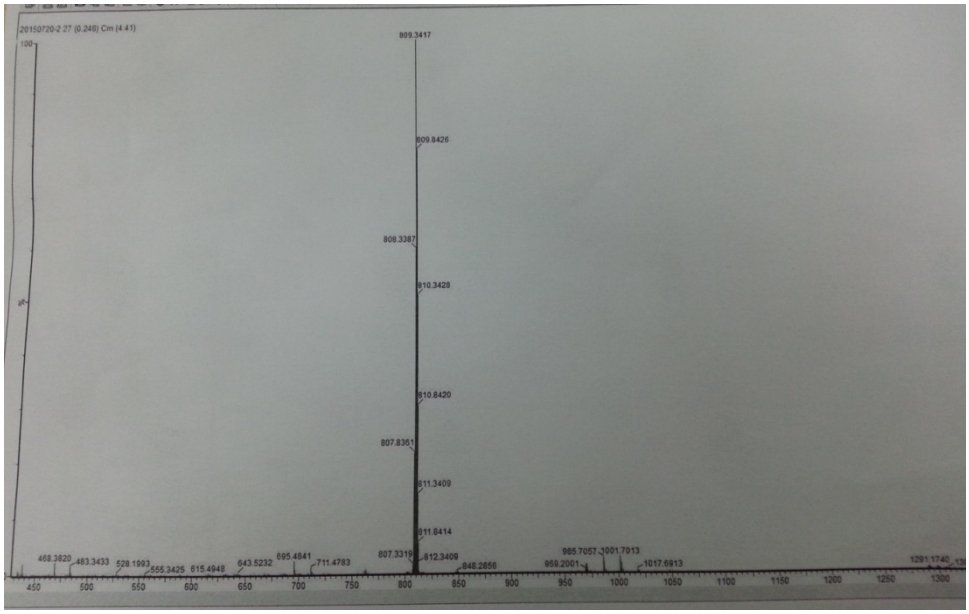

**Figure S30.** Electrospray ionization spectrum of compound **1**.

## *14.3 Synthesis of compound **3***

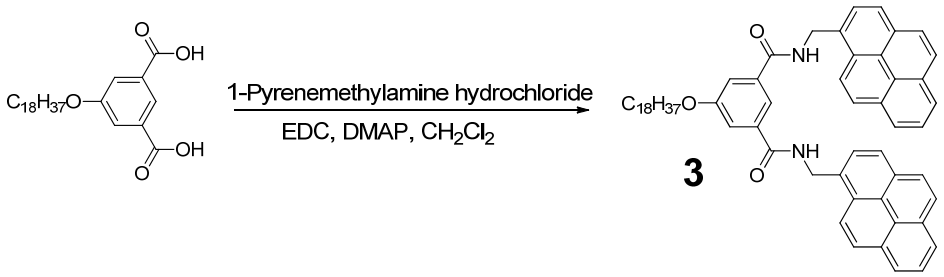


5-Octadecyloxyisophthalic acid (600 mg, 1.38 mmol), EDC·HCl (1.50 g, 8.00 mmol), 1-pyrenylmethylamine hydrochloride (800 mg, 3.00 mmol) and DMAP (40 mg, 0.32 mmol) were dissolved in 150 mL of $CH_2Cl_2$ and stirred at room temperature for 72 hours. After the reaction was complete, the mixture was extracted with $H_2O/CH_2Cl_2$. The combined organic extracts were removed with a rotary evaporator and the residue was purified by flash column chromatography ($CH_3OH/CH_2Cl_2$, 1 : 100 *v*/*v* as the eluent) to provide compound **3** as a white solid (830 mg, 70%). Mp: 188.5−189.9 $^{o}$C. $^{1}$H NMR (300 MHz, $CDCl_3$, room temperature) $\delta$ (ppm): 8.27–8.08 (m, 7H), 8.08–7.90 (m, 11H), 7.85 (d, $J$ = 8 Hz, 2H), 7.56 (s, 1H), 6.57 (t, $J$ = 5 Hz, 2H), 5.17 (d, $J$ = 5 Hz, 4H), 3.82 (t, $J$ = 6 Hz, 2H), 1.73–1.61 (m, 2H), 1.25 (m, 30H), 0.88 (t, $J$ = 7 Hz, 3H). $^{13}$C NMR (100 MHz, $CDCl_3$, room temperature) $\delta$ (ppm): 165.9, 159.3, 135.2, 131.2, 131.1, 130.6, 130.5, 129.0, 128.3, 127.6, 127.2, 126.1, 125.4, 124.9, 124.7, 124.6, 122.6, 116.5, 116.2, 68.4, 42.5, 31.9, 29.7, 29.6, 29.4, 22.7, 14.1. TOF-MS *m*/*z*: calcd for $[M + H]^+$, $C_{60}H_{65}N_2O_3$, 861.4995; found, 861.6630.

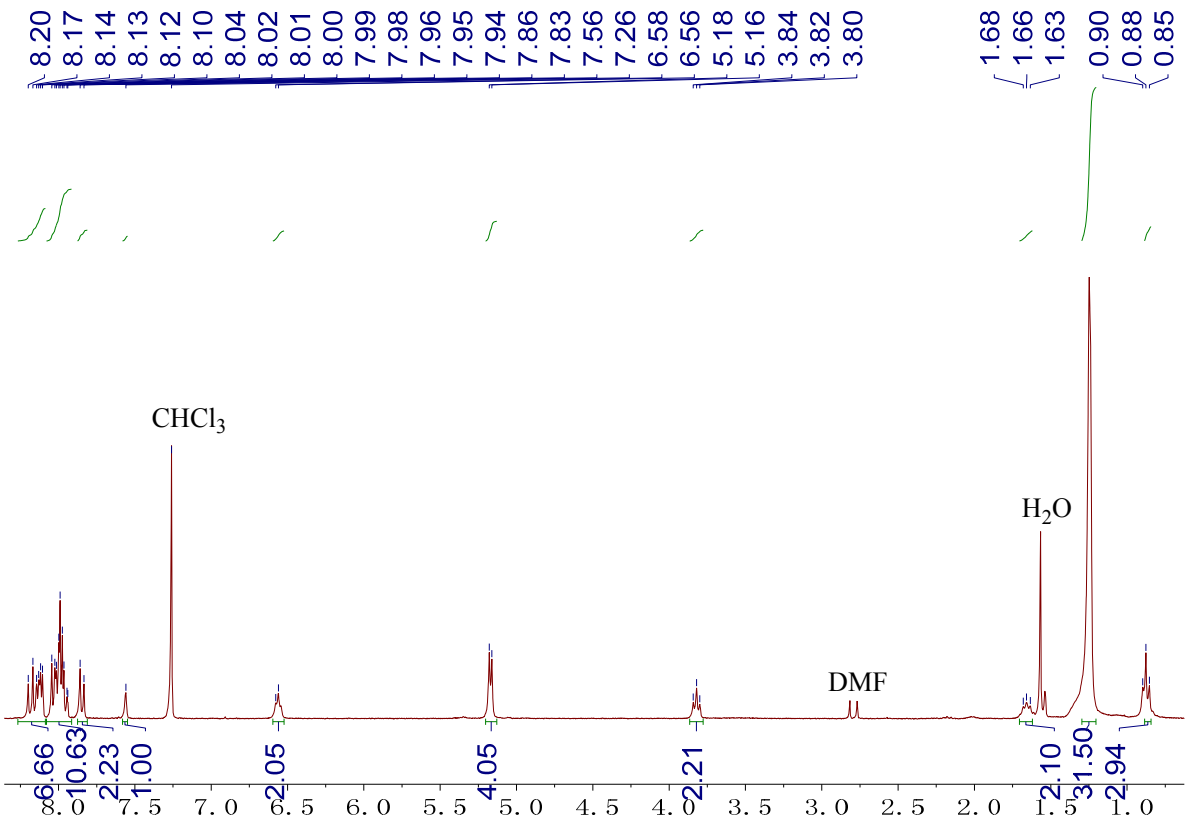


**Figure S31.** $^{1}$H NMR spectrum (300 MHz, $CDCl_3$, room temperature) of **3**.

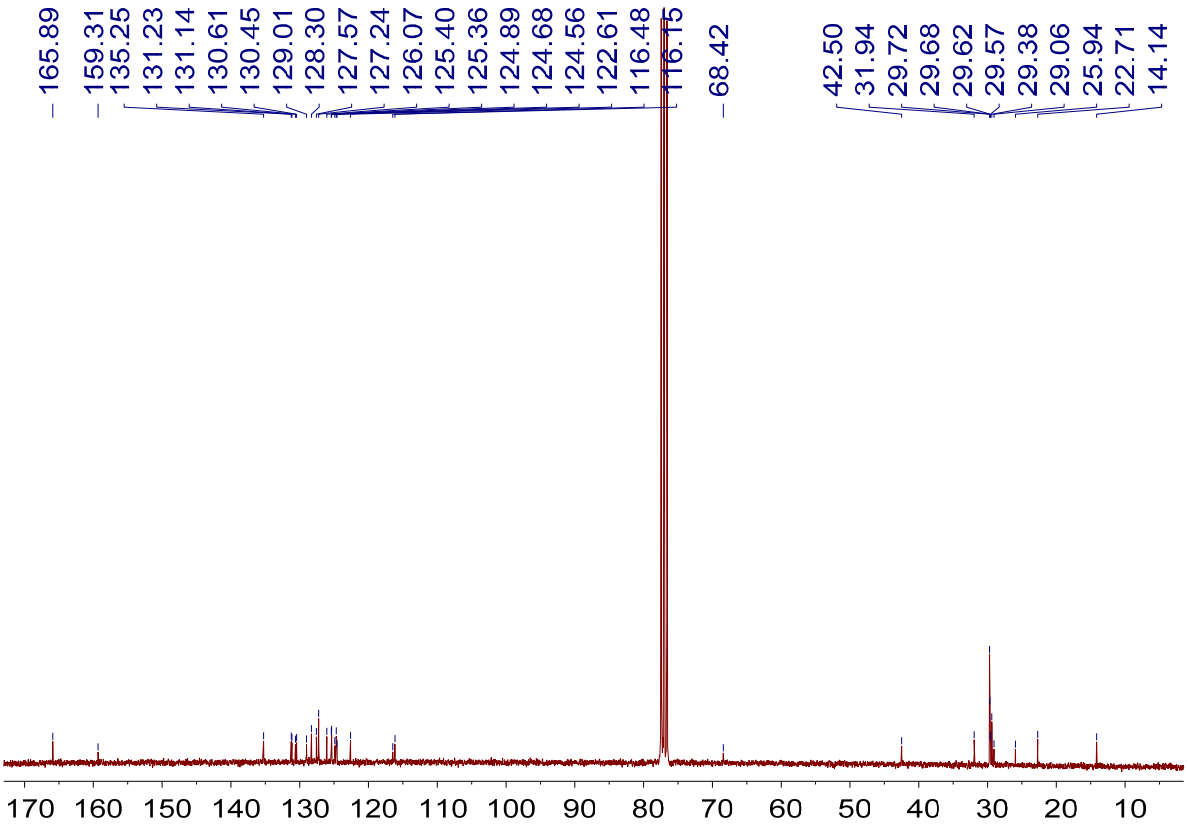


**Figure S32.** $^{13}$C NMR spectrum (75 MHz, $CDCl_3$, room temperature) of **3**.

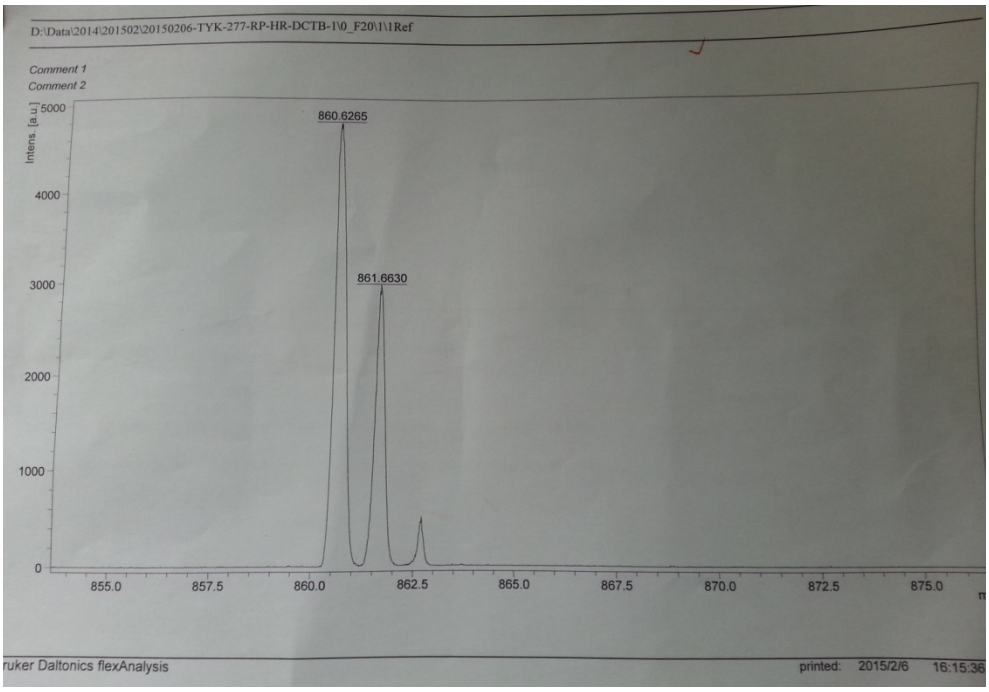


**Figure S33.** MALDI-TOF spectrum of **3**.

## *15. Synthetic routes to the homoditopic monomers **4**, **5** and **8***

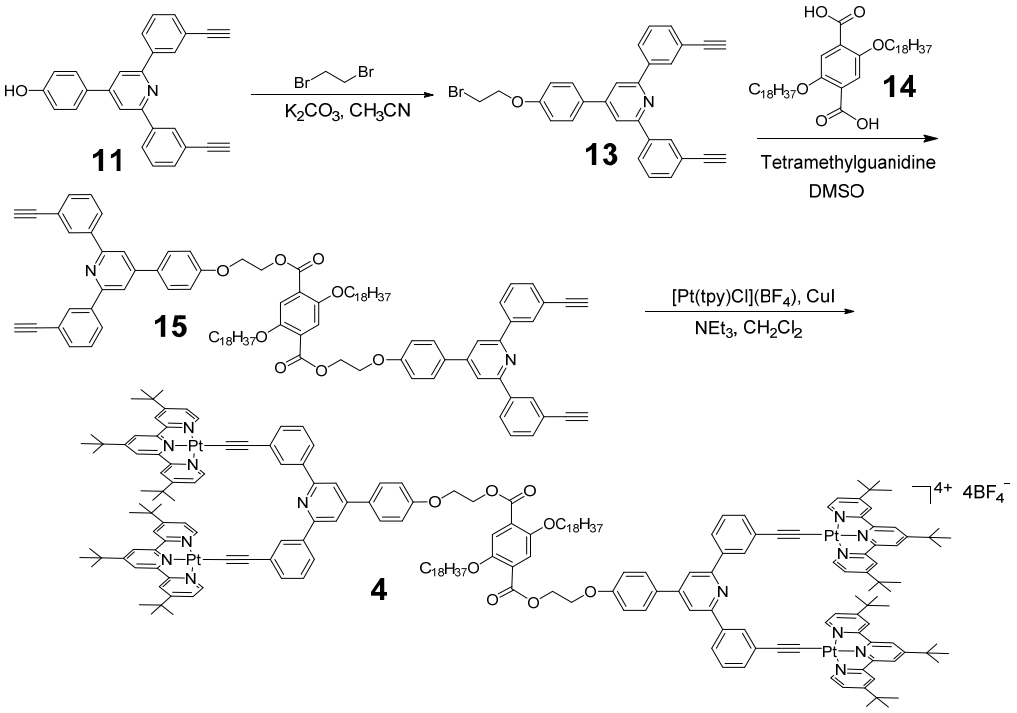


**Figure S34.** Synthetic routes to the homoditopic monomer **4**.

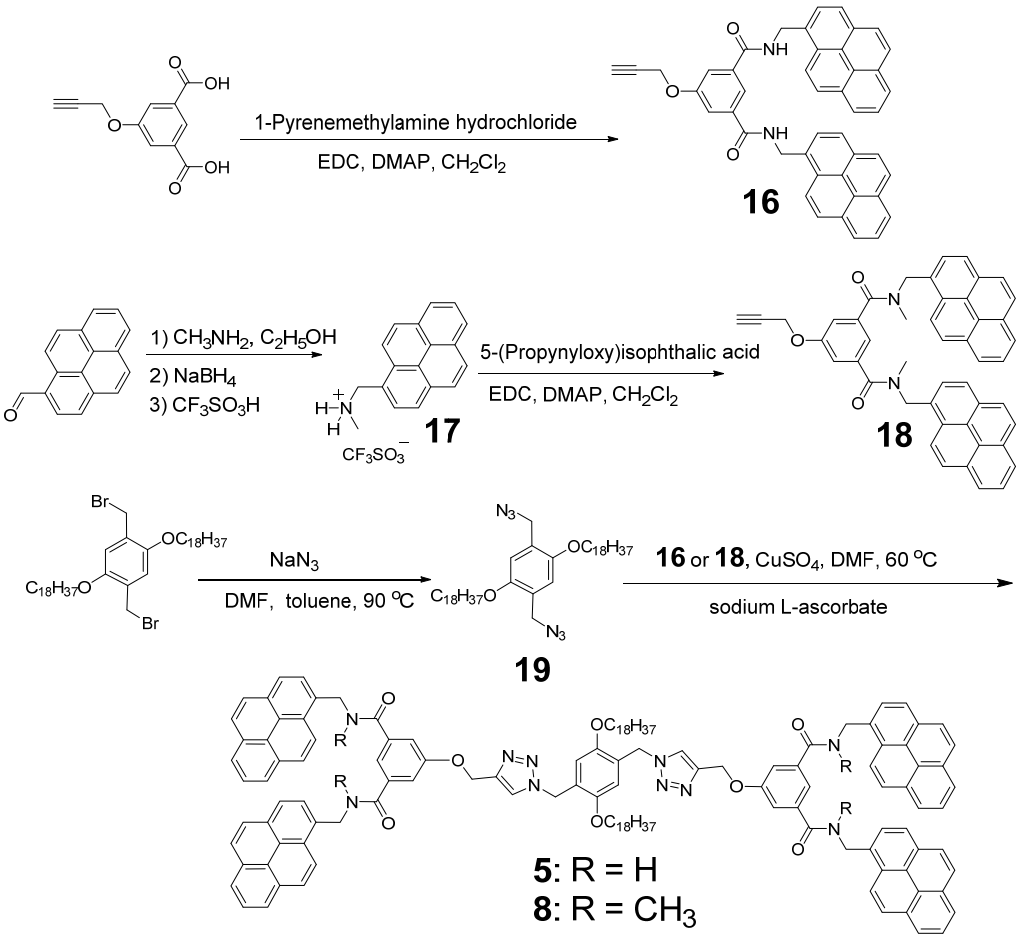


**Figure S35.** Synthetic routes to the homoditopic monomers **5** and **8**.

## *15.1 Synthesis of compound **15***

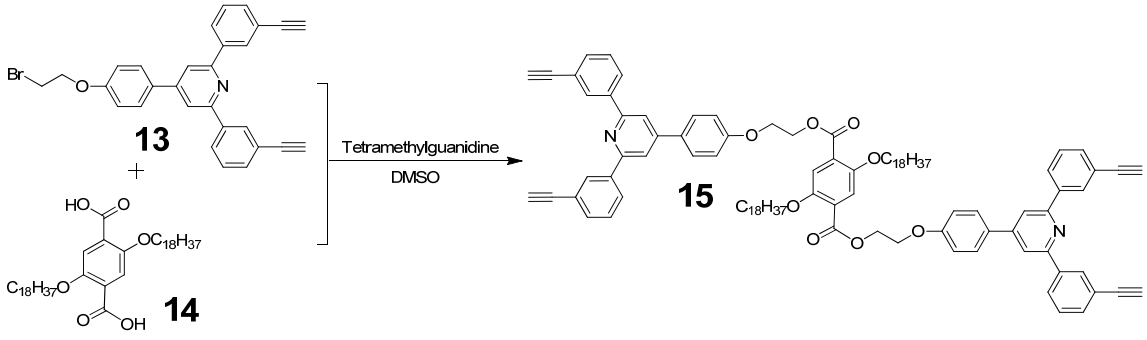


Compounds **13** (3.00 g, 6.29 mmol), **14** (2.00 g, 2.86 mmol) and tetramethylguanidine (1.00 g, 8.58 mmol) were dissolved in DMSO (50 mL) and stirred at 60 $^{o}$C for 36 hours. After the reaction was complete, the mixture was extracted with $H_2O/CH_2Cl_2$. The combined organic extracts were dried over anhydrous $Na_2SO_4$ and evaporated with a rotary evaporator. The residue was purified by flash column chromatography (petroleum ether/$CH_2Cl_2$, 2 : 1 *v*/*v* as the eluent) to afford **15** as a white solid (3.08 g, 72%). Mp: 103.5−104.8 $^{o}$C. $^{1}$H NMR (300 MHz, $CDCl_3$, room temperature) $\delta$ (ppm): 8.22 (s, 4H), 8.13 (d, $J$ = 8 Hz, 4H), 7.78 (s, 4H), 7.64 (d, $J$ = 9 Hz, 4H), 7.51 (d, $J$ = 8 Hz, 4H), 7.41 (t, $J$ = 8 Hz, 4H), 7.33 (s, 2H), 7.01 (d, $J$ = 9 Hz, 4H), 4.70–4.57 (m, 4H), 4.36–4.23 (m, 4H), 3.91 (t, $J$ = 7 Hz, 4H), 3.07 (s, 4H), 1.72–1.61 (m, 4H), 1.31 (s, 4H), 1.20–1.15 (m, 56H), 0.84–0.80 (m, 6H). $^{13}$C NMR (75 MHz, $CDCl_3$, room temperature) $\delta$ (ppm): 165.9, 159.6, 156.6, 152.0, 149.7, 139.7, 132.7, 131.3, 130.7, 128.8, 128.4, 127.7, 124.2, 122.6, 116.8, 115.2, 83.7, 70.0, 66.1, 63.5, 31.9, 30.9, 29.7, 29.4, 29.3, 26.0, 22.7, 14.1. ESI–MS *m*/*z*: calcd for $[M + H]^+$, $C_{102}H_{117}N_2O_8$, 1497.8810; found, 1497.8524.

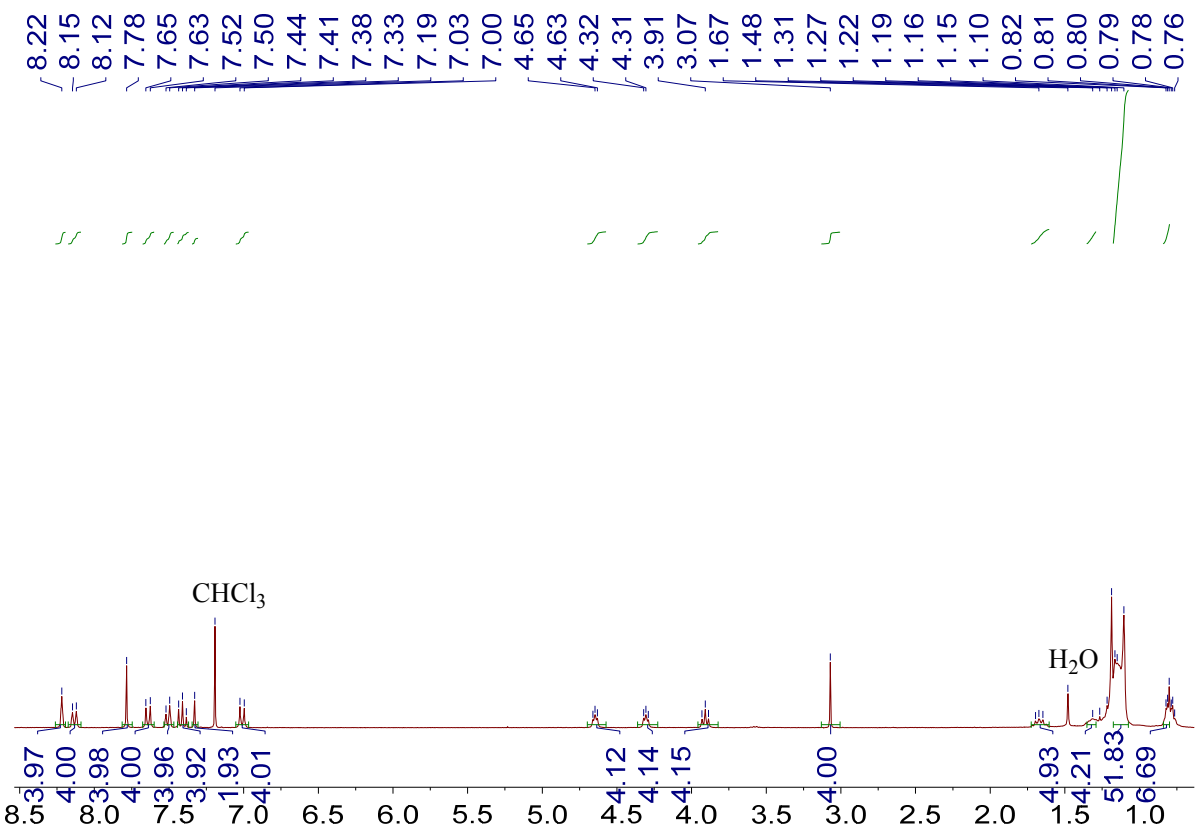


**Figure S36.** $^{1}$H NMR spectrum (300 MHz, $CDCl_3$, room temperature) of compound **15**.

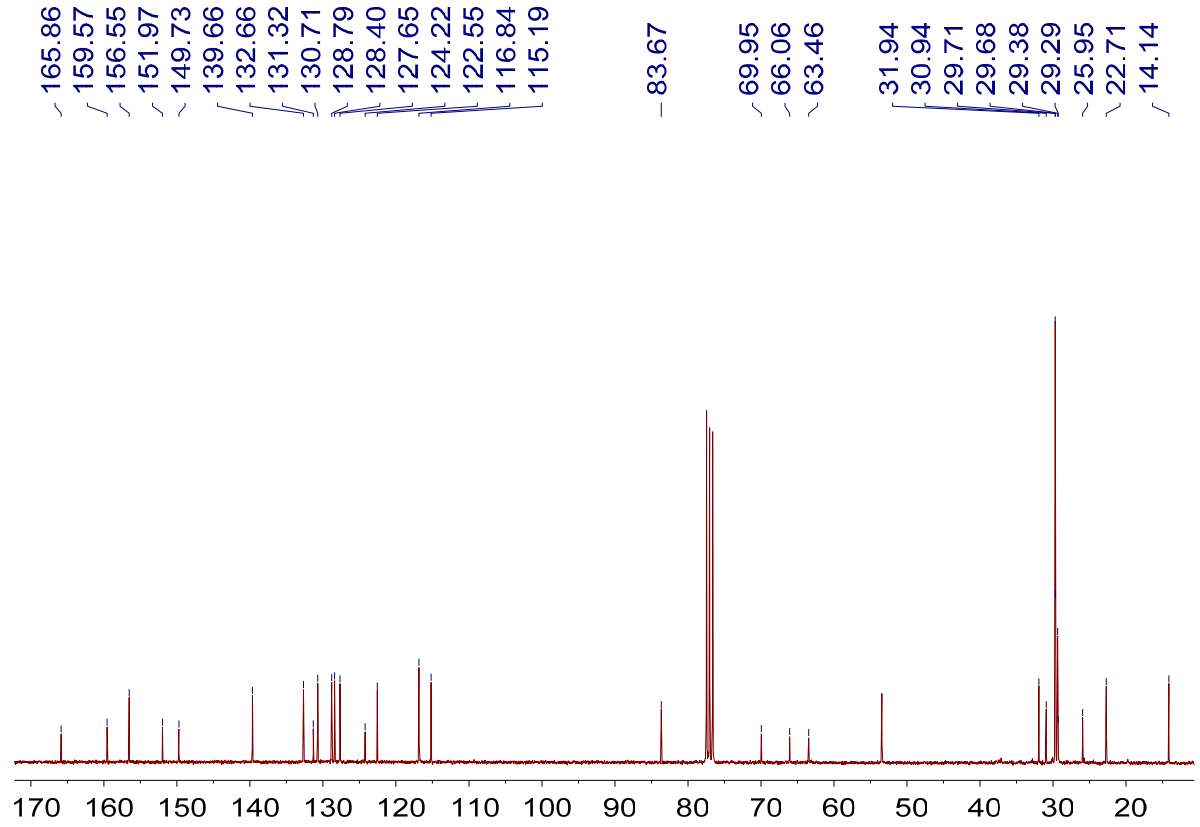


**Figure S37.** $^{13}$C NMR spectrum (75 MHz, $CDCl_3$, room temperature) of compound **15**.

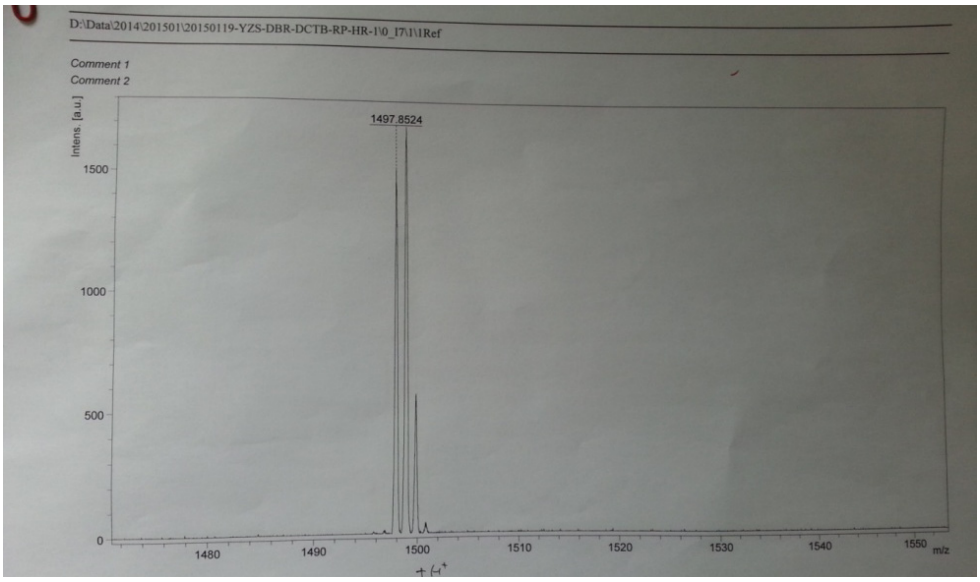


**Figure S38.** Electrospray ionization spectrum of compound **15**.

## *15.2 Synthesis of monomer **4***

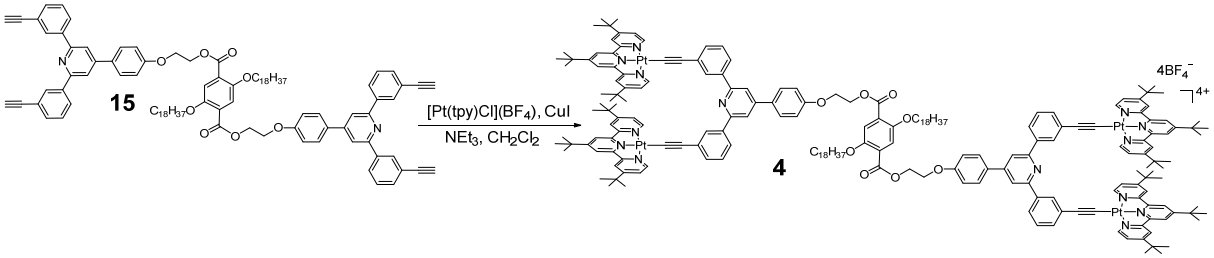


Compound **15** (890 mg, 0.60 mmol), [Pt(tpy)Cl](BF$_4$) (2.15 g, 3.00 mmol), CuI (50 mg, 0.25 mmol) and $NEt_3$ (20 mL) in 200 mL of $CH_2Cl_2$ were stirred at room temperature for 48 hours. The mixture was evaporated under reduced pressure and the residue was purified by column chromatography (alumina, $CH_3OH/CH_2Cl_2$, 100 : 1 *v*/*v* as the eluent) to afford **4** as a reddish-brown solid (1.87 g, 74%). The compound **4** began to decompose before reaching the melting point. $^1$H NMR (300 MHz, $CDCl_3$, room temperature) $\delta$ (ppm): 9.02 (s, 8H), 8.79 (s, 8H), 8.72 (s, 8H), 8.46 (s, 4H), 7.91 (s, 4H), 7.81 (s, 4H), 7.70 (d, $J$ = 7 Hz, 4H), 7.50 (m, 12H), 7.36 (s, 4H), 7.30 (s, 2H), 7.03 (d, $J$ = 9 Hz, 4H), 4.65 (s, 4H), 4.34 (s, 4H), 3.92 (t, $J$ = 6 Hz, 4H), 1.60 (m, 36H), 1.48 (m, 72H), 1.18 (m, 64H), 0.83 (t, $J$ = 7 Hz, 6H). $^{13}$C NMR (100 MHz, $CDCl_3$, room temperature) $\delta$ (ppm): 168.5, 167.2, 159.6, 158.7, 156.6, 153.8, 153.7, 152.0, 139.2, 132.6, 130.6, 128.6, 128.3, 127.3, 125.1, 124.0, 122.3, 116.9, 115.4, 104.2, 98.7, 70.0, 66.0, 63.5, 37.8, 36.6, 31.9, 30.9, 30.5, 29.7, 29.4, 26.0, 22.7, 14.2. ESI–MS *m*/*z*: calcd for $[M - 4BF_4]^{4+}$, $C_{210}H_{252}N_{14}O_8Pt_4$, 969.4584; found, 969.4452.

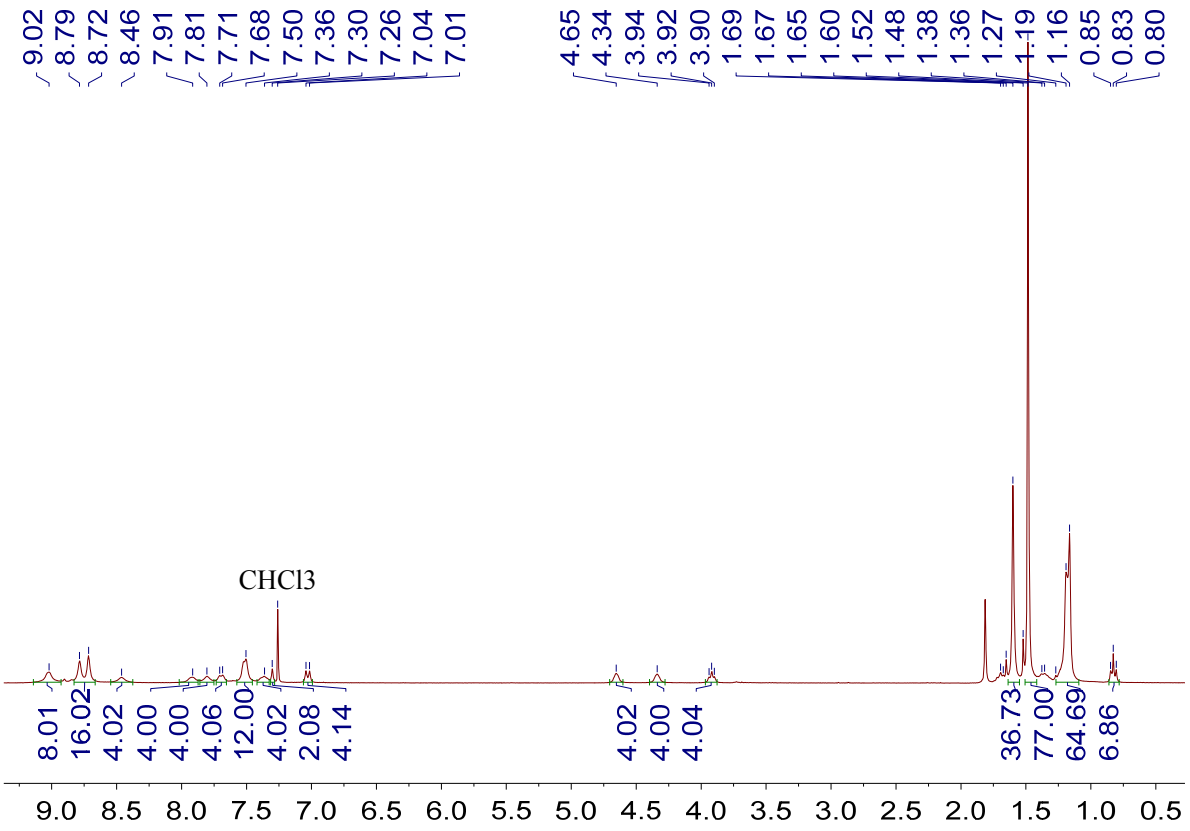


**Figure S39.** $^{1}$H NMR spectrum (300 MHz, $CDCl_3$, room temperature) of **4**.

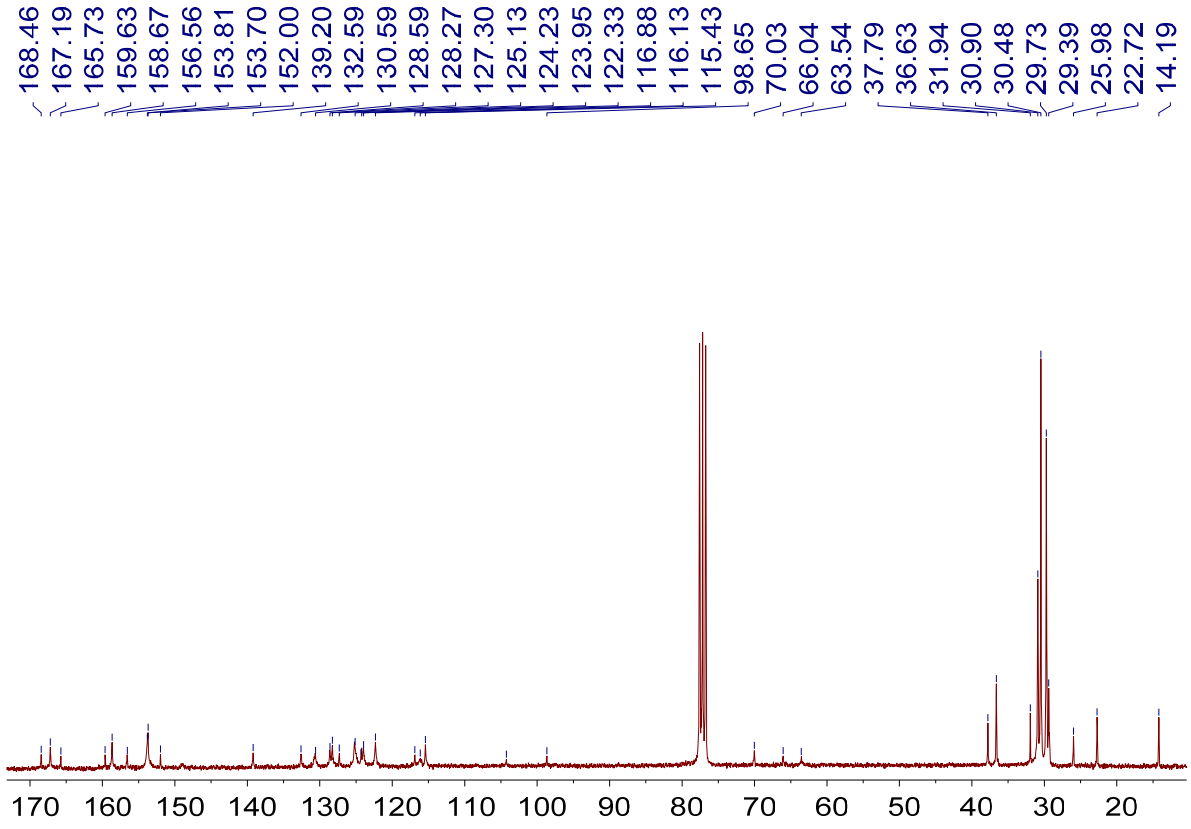


**Figure S40.** $^{13}$C NMR spectrum (100 MHz, $CDCl_3$, room temperature) of **4**.

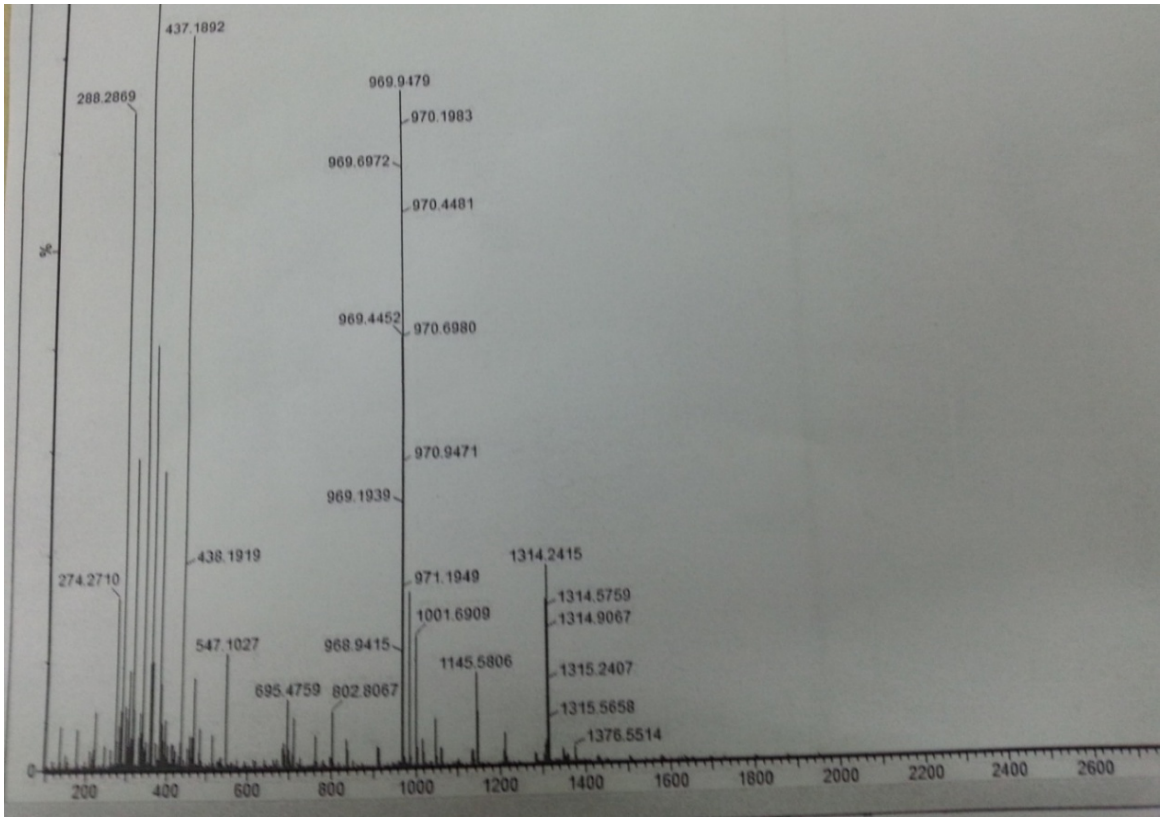


**Figure S41.** Electrospray ionization spectrum of **4**.

## *15.3 Synthesis of compound **16***

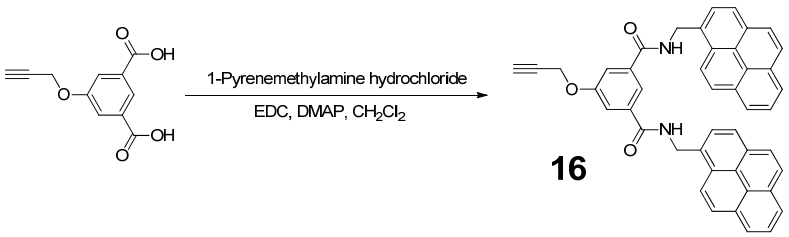


5-Propargyloxyisophthalic acid (1.00 g, 4.55 mmol), 1-pyrenylmethylamine hydrochloride (2.68 g, 10.0 mmol), EDC·HCl (3.80 g, 20.0 mmol) and DMAP (20 mg, 0.16 mmol) were dissolved in 200 mL of $CH_2Cl_2$, and the mixture was stirred at room temperature for 72 hours. After the reaction was complete, the mixture was extracted with $H_2O/CH_2Cl_2$. The combined organic extracts were removed with a rotary evaporator and the residue was purified by flash column chromatography ($CH_3OH/CH_2Cl_2$, 1 : 100 *v*/*v* as the eluent) to provide **16** as a white solid (1.92 g, 65%). Mp: 166.3−168.7 $^{o}$C. $^{1}$H NMR (300 MHz, DMSO-$d_6$, room temperature) $\delta$(ppm): 9.35 (t, $J$ = 6 Hz, 2H), 8.50 (d, $J$ = 9 Hz, 2H), 8.37–8.21 (m, 8H), 8.20–8.00 (m, 9H), 7.71 (s, 2H), 5.24 (d, $J$ = 6 Hz, 4H), 4.90 (d, $J$ = 2 Hz, 2H), 3.60 (s, 1H). $^{13}$C NMR (100 MHz, DMSO-$d_6$, room temperature) $\delta$ (ppm): 165.7, 157.4, 136.2, 133.0, 131.0, 130.5, 130.4, 128.4, 127.8, 127.6, 127.3, 127.0, 126.5, 125.5, 125.4, 124.9, 124.3, 124.2, 123.5, 119.8, 116.8, 79.0, 78.9, 56.2, 41.4. ESI–MS *m*/*z*: calcd for $[M + Na]^+$, $NaC_{45}H_{30}N_2O_3$, 669.2154; found,

669.2147.

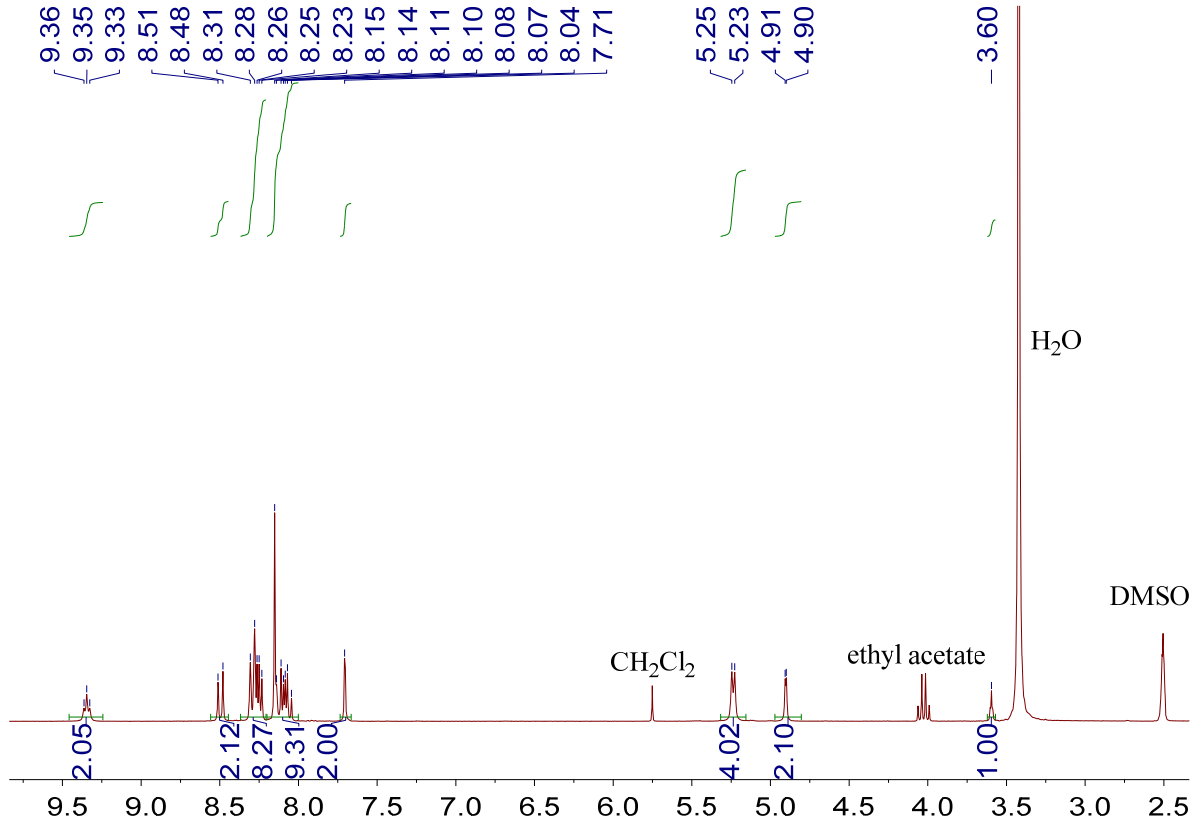


**Figure S42.** $^{1}$H NMR spectrum (300 MHz, DMSO-$d_6$, room temperature) of compound **16**.

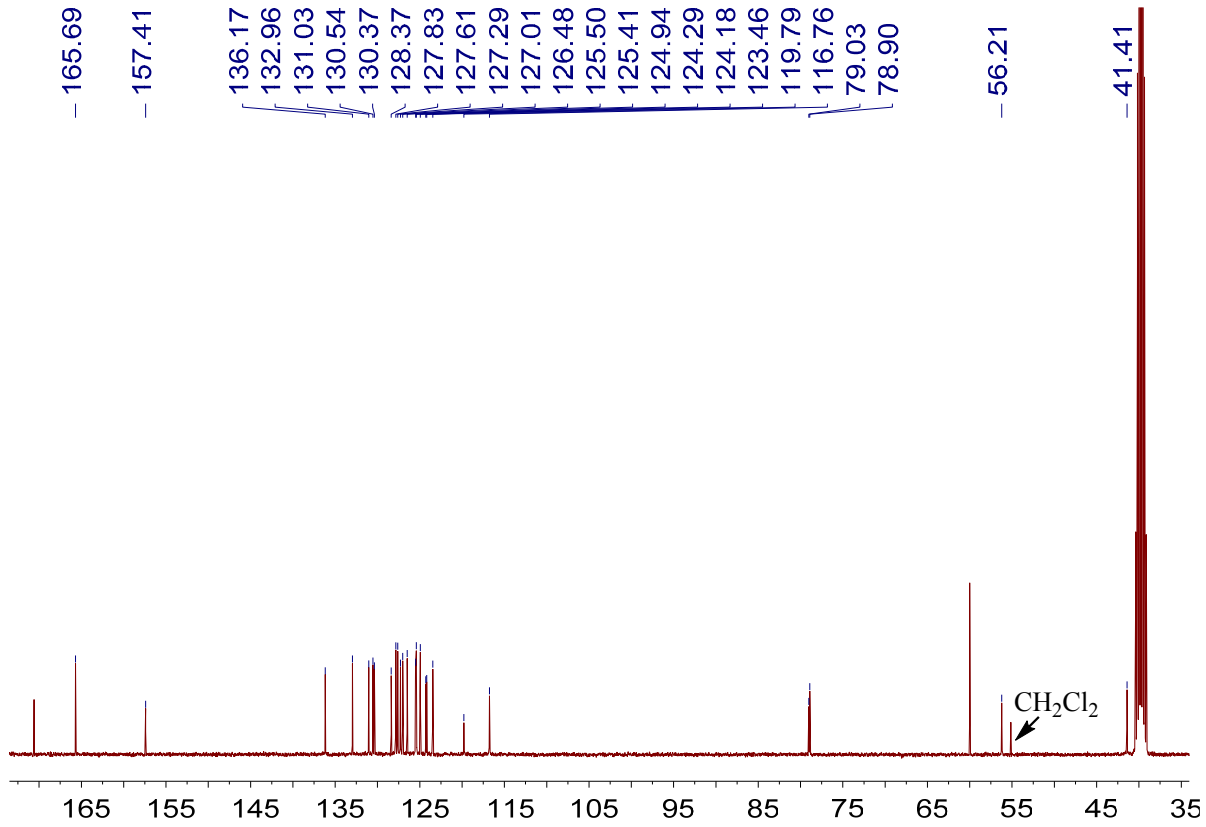


**Figure S43.** $^{13}$C NMR spectrum (100 MHz, DMSO-$d_6$, room temperature) of compound **16**.

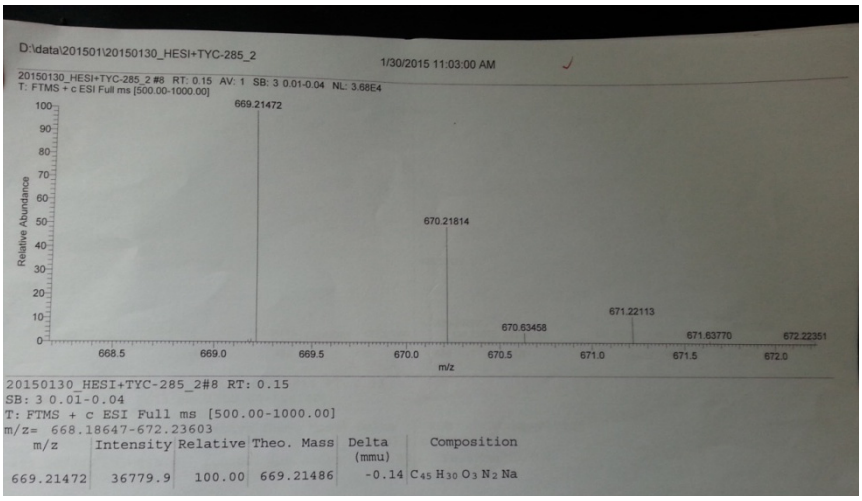


**Figure S44.** Electrospray ionization spectrum of compound **16**.

## *15.4 Synthesis of monomer **5***

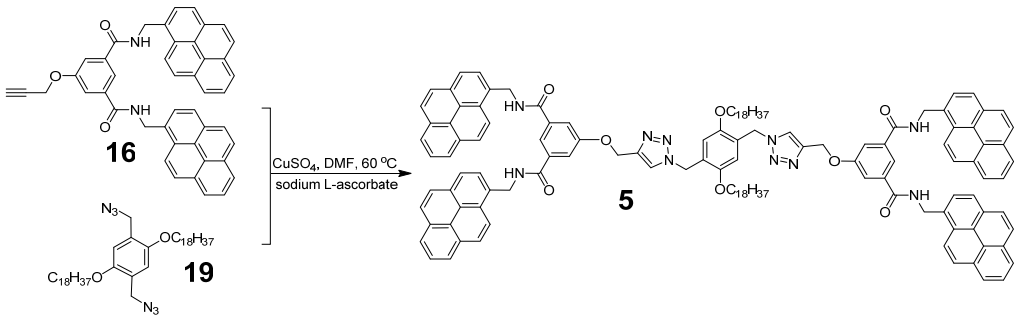


Compounds **16** (500 mg, 0.77 mmol) and **19** (250 mg, 0.35 mmol) were dissolved in 50 mL of DMF. An aqueous solution (15 mL) of monosodium L-ascorbate (400 mg, 2.02 mmol) and $CuSO_4 \cdot 5H_2O$ (50 mg, 0.20 mmol) was then added. The resulting mixture was heated at 60 °C and stirred for 48 hours. The solvent was then removed with a rotary evaporator and the residue was extracted with $H_2O/CH_2Cl_2$. The combined organic extracts were dried over anhydrous $Na_2SO_4$ and removed with a rotary evaporator. The crude product was purified by flash column chromatography ($CH_2Cl_2/CH_3OH$, 200 : 1 *v*/*v* as the eluent) to afford **5** as a white solid (390 mg, 55%). Mp: 175.2−177.4 °C. $^1$H NMR (300 MHz, $CDCl_3$, room temperature) $\delta$ (ppm): 8.05–7.98 (m, 8H), 7.96–7.89 (m, 6H), 7.87 (d, $J$ = 2 Hz, 4H), 7.85–7.76 (m, 14H), 7.56 (d, $J$ = 8 Hz, 4H), 7.43 (s, 2H), 7.31 (s, 2H), 7.00 (s, 4H), 6.66 (m, 6H), 5.42 (s, 4H), 4.88 (d, $J$ = 5 Hz, 8H), 4.78 (s, 4H), 3.80 (t, $J$ = 6 Hz, 4H), 2.02 (s, 4H), 1.68 (d, $J$ = 7 Hz, 4H), 1.39–1.11 (m, 56H), 0.86 (t, $J$ = 6 Hz, 6H). $^{13}$C NMR (100 MHz, $CDCl_3$, room temperature) $\delta$ (ppm): 165.5, 157.7, 150.3, 143.2, 134.6, 131.0, 130.9, 130.4, 128.7, 128.0, 127.3, 127.1, 126.9, 125.9, 125.2, 124.6, 124.4, 124.2, 123.1, 122.5, 116.7, 116.3, 114.0, 68.9, 61.4, 48.9, 42.1, 31.9, 29.7, 29.6, 29.4, 29.3, 29.2, 26.0, 22.7, 14.1. TOF-MS *m*/*z*: calcd for $[M + Na]^+$, $C_{134}H_{140}N_{10}O_8Na$, 2040.0753; found, 2040.1272.

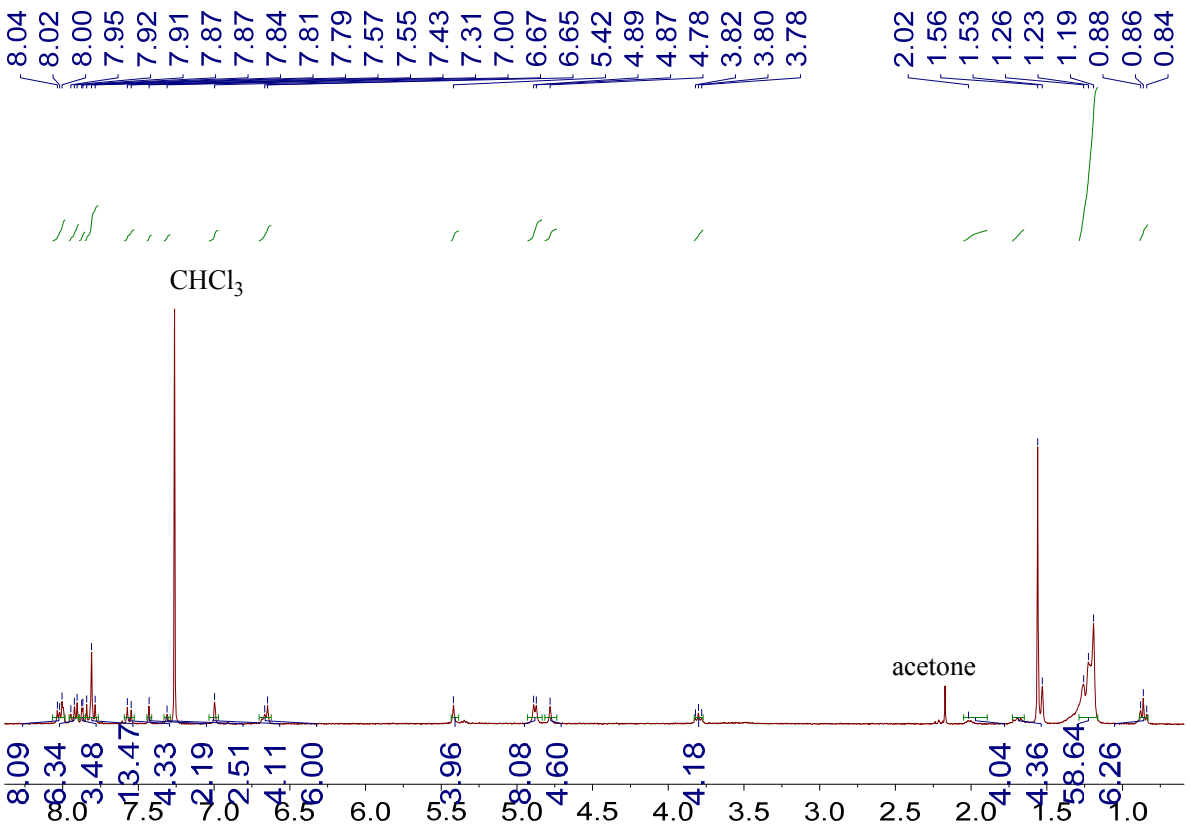


**Figure S45.** $^{1}$H NMR spectrum (300 MHz, $CDCl_3$, room temperature) of **5**.

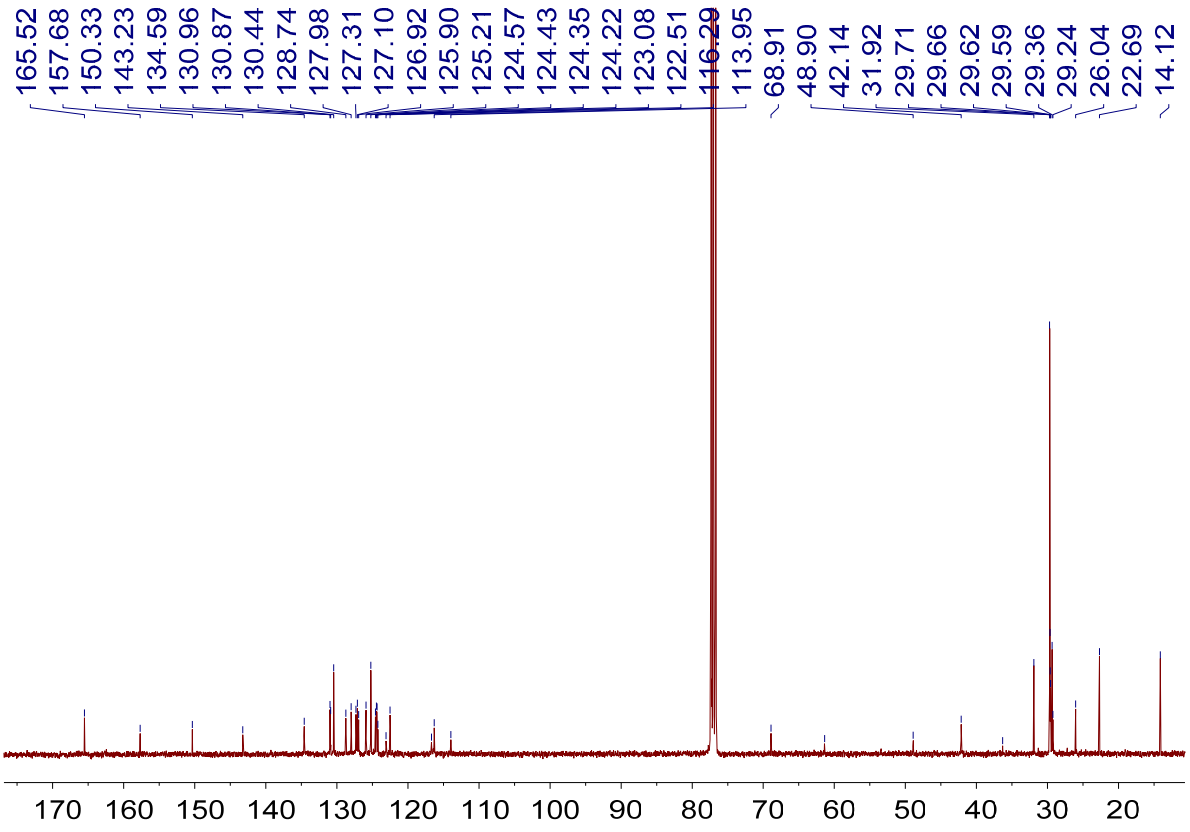


**Figure S46.** $^{13}$C NMR spectrum (100 MHz, $CDCl_3$, room temperature) of **5**.

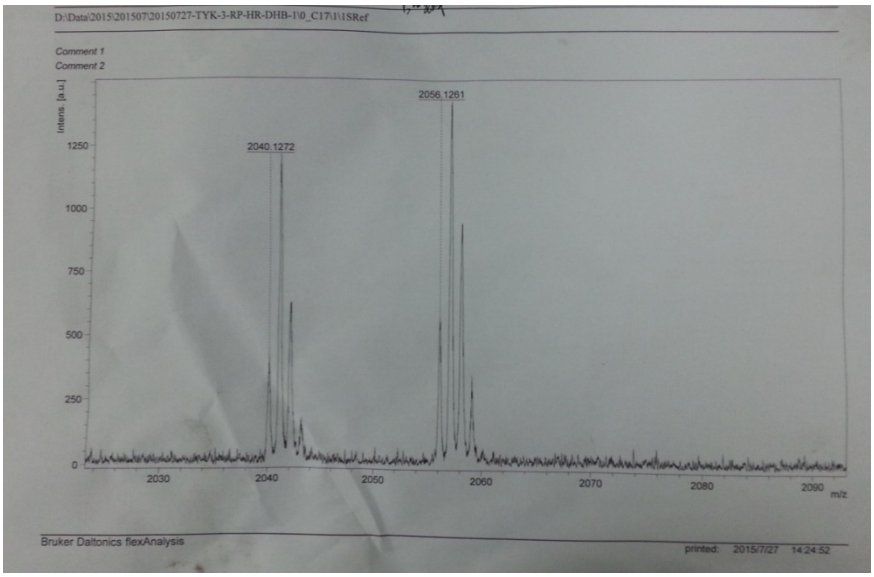


**Figure S47.** MALDI-TOF spectrum of **5**.

## *15.5 Synthesis of compound **17***

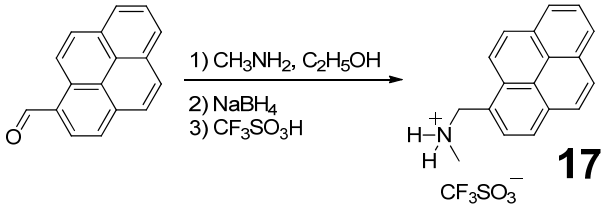


1-Pyrenecarboxaldehyde (2.30 g, 10.0 mmol) and methylamine (33% in $C_2H_5OH$, 100 mL) were stirred at room temperature for 6 hours. $NaBH_4$ was then added to the solution at 0 °C and the resulting mixture was stirred at room temperature overnight. After the reaction was complete, the solvent was evaporated under reduced pressure and the residue was extracted with $H_2O/CH_2Cl_2$. The combined organic extracts were dried over anhydrous $Na_2SO_4$ and purified by flash column chromatography ($CH_3OH/CH_2Cl_2$, 40 : 1 *v*/*v* as the eluent) to afford the crude product as a colorless oil. It was further dissolved in $CH_2Cl_2$ and 2 mL of $CF_3SO_3H$ was added. The precipitated product was filtered and washed with $CH_2Cl_2$ to afford **17** as a yellow solid (2.00 g, 51%). Mp: 246.5−248.3 °C. $^1$H NMR (300 MHz, DMSO-$d_6$, room temperature) $\delta$ (ppm): 8.91 (s, 2H), 8.58 (d, $J$ = 9 Hz, 1H), 8.44–8.35 (m, 4H), 8.25 (m, 3H), 8.15 (m, 1H), 4.95 (s, 2H), 2.76 (s, 3H). $^{13}$C NMR (75 MHz, DMSO-$d_6$, room temperature) $\delta$ (ppm): 131.5, 130.7, 130.2, 129.3, 129.0, 128.3, 128.2, 127.2, 126.6, 125.9, 125.7, 125.5, 124.8, 123.9, 123.6, 123.1, 48.5, 32.8, 30.6. ESI–MS *m*/*z*: calcd for $[M - CF_3SO_3]^+$, $C_{18}H_{16}N$, 246.12; found, 246.11.

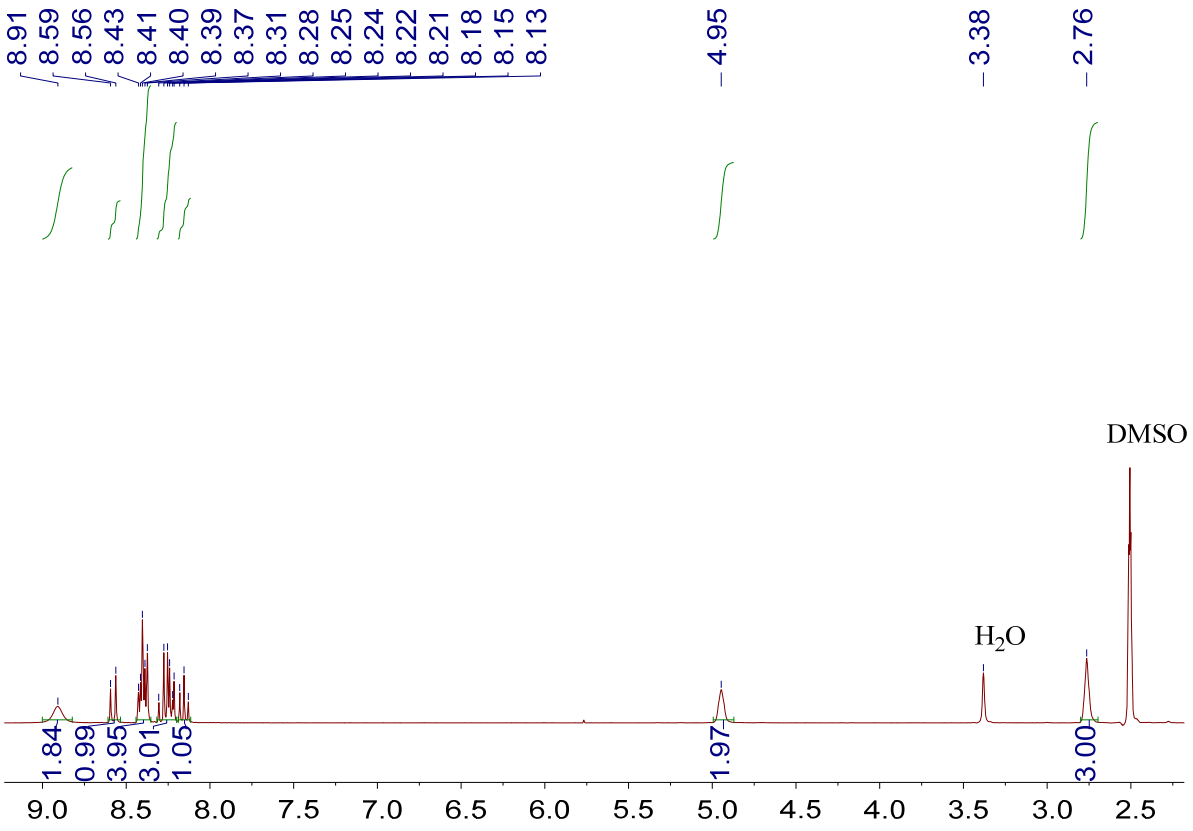


**Figure S48.** $^{1}$H NMR spectrum (300 MHz, DMSO-$d_6$, room temperature) of compound **17**.

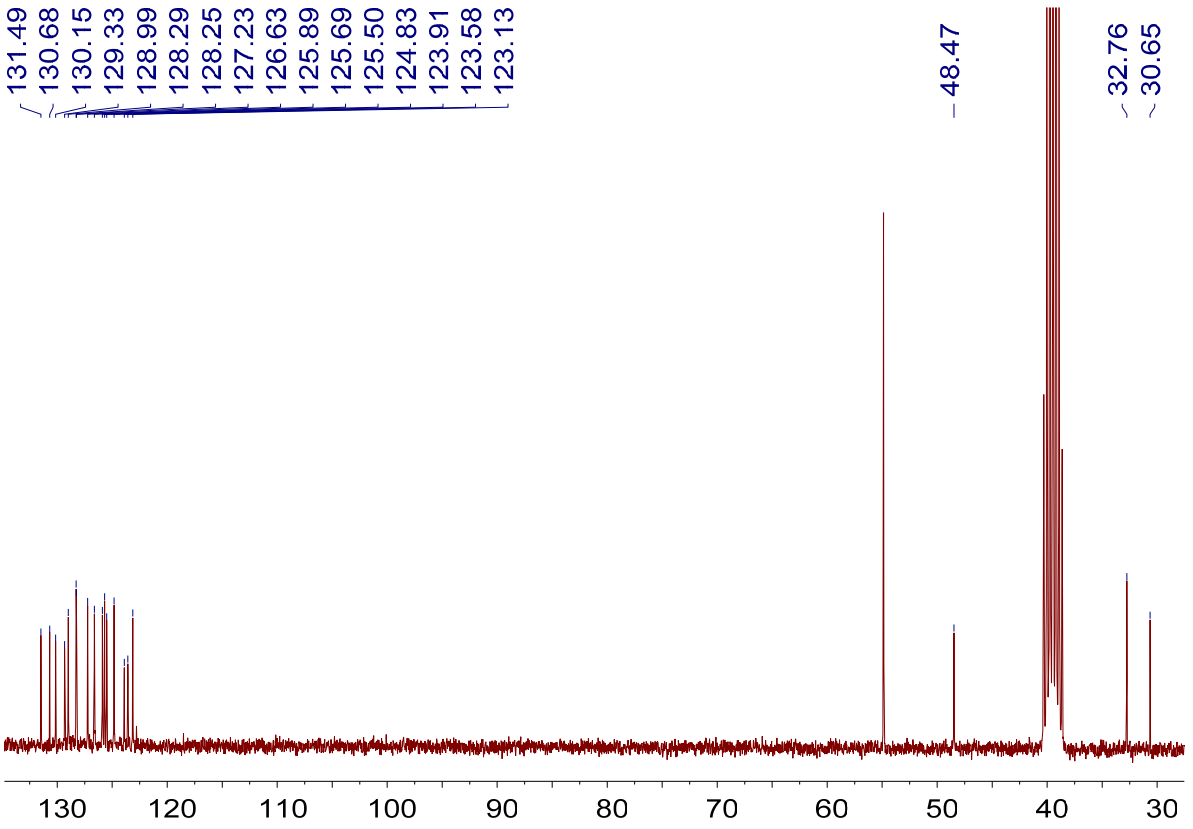


**Figure S49.** $^{13}$C NMR spectrum (75 MHz, DMSO-$d_6$, room temperature) of compound **17**.

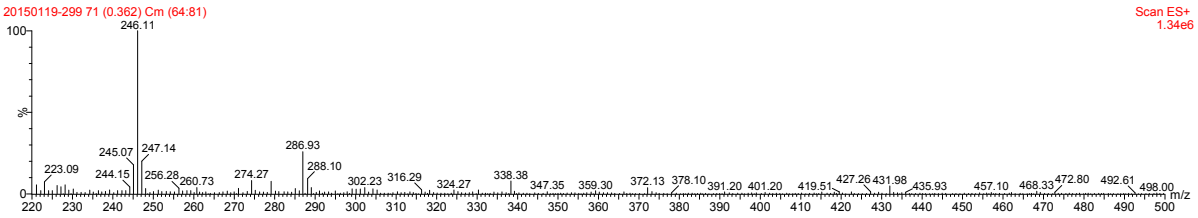


**Figure S50.** Electrospray ionization spectrum of compound **17**.

## *15.6 Synthesis of monomer **8***

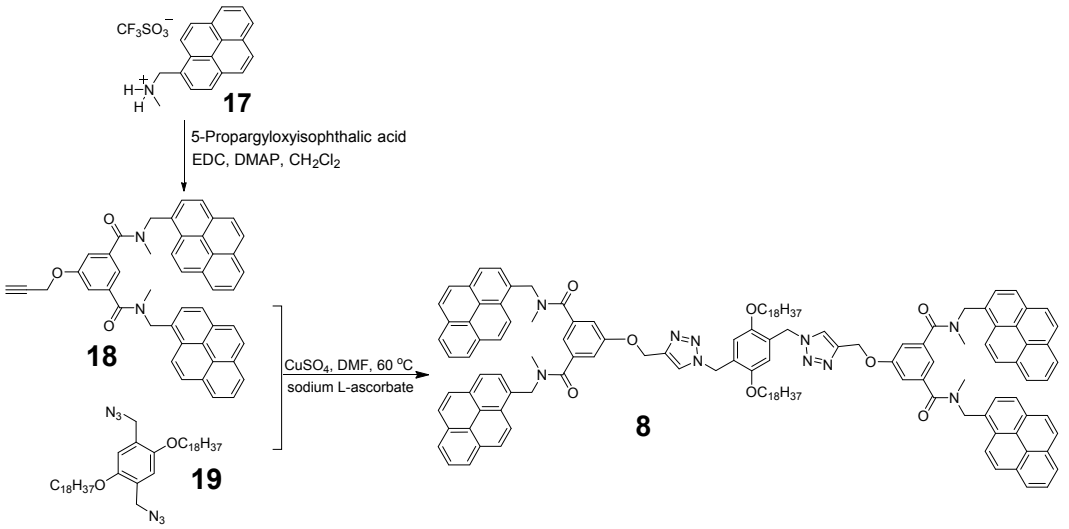


Compound **17** (3.56 g, 9.00 mmol), 5-propargyloxyisophthalic acid (880 mg, 4.00 mmol), EDC·HCl (3.00 g, 15.8 mmol) and DMAP (200 mg, 1.60 mmol) were dissolved in 100 mL of $CH_2Cl_2$ and stirred at room temperature for 24 hours. After the reaction was complete, the mixture was extracted with $H_2O/CH_2Cl_2$. The combined organic extracts were removed with a rotary evaporator and the residue was purified by flash column chromatography (acetone/$CH_2Cl_2$, 1 : 100 *v*/*v* as the eluent) to provide **18** as a yellow solid (1.97 g, 73%). Compounds **18** (800 mg, 1.18 mmol) and **19** (360 mg, 0.50 mmol) were then dissolved in 60 mL of DMF. An aqueous solution (15 mL) of monosodium L-ascorbate (500 mg, 2.50 mmol) and $CuSO_4$•$5H_2O$ (50 mg, 0.20 mmol) was added. The resulting mixture was heated at 60 °C and stirred for 48 hours. The solvent was then removed with a rotary evaporator and the residue was extracted with $H_2O/CH_2Cl_2$. The combined organic extracts were dried over anhydrous $Na_2SO_4$ and removed with a rotary evaporator. The crude product was purified by flash column chromatography ($CH_2Cl_2/CH_3OH$, 200 : 1 *v*/*v* as the eluent) to afford **8** as a yellow solid (720 mg, 70%). Mp: 104.7−106.8 °C. The $^1$H NMR spectrum of compound **8** shows broadened and ill-resolved peaks. With reference to the previous literatures,[S11] it should be ascribed to the carbon−nitrogen bond rotation of the asymmetrical molecule, leading to severe peak splitting phenomenon. $^1$H NMR (300 MHz, $CDCl_3$, room temperature) $\delta$ (ppm):

8.54–7.29 (m, 38H), 7.18–7.01 (m, 6H), 6.80–6.60 (s, 2H), 5.39 (m, 8H), 5.22–4.55 (m, 8H), 3.77 (m, 4H), 3.18–2.20 (m, 12H), 1.72–1.52 (m, 8H), 1.22 (s, 56H), 0.86 (t, $J$ = 6.6 Hz, 6H). $^{13}$C NMR (100 MHz, $CDCl_3$, room temperature) $\delta$ (ppm): 170.0, 158.4, 150.4, 143.2, 138.1, 131.2, 130.8, 129.4, 128.2, 127.5, 127.3, 126.1, 125.4, 125.0, 124.7, 124.2, 123.2, 122.9, 121.3, 117.8, 114.0, 68.9, 62.1, 53.4, 49.0, 36.7, 31.9, 30.9, 29.7, 29.6, 29.4, 29.2, 26.0, 22.7, 14.1. ESI–MS $m/z$: calcd for $[M + H]^+$, $C_{138}H_{149}N_{10}O_8$, 2074.1560; found, 2074.1614.

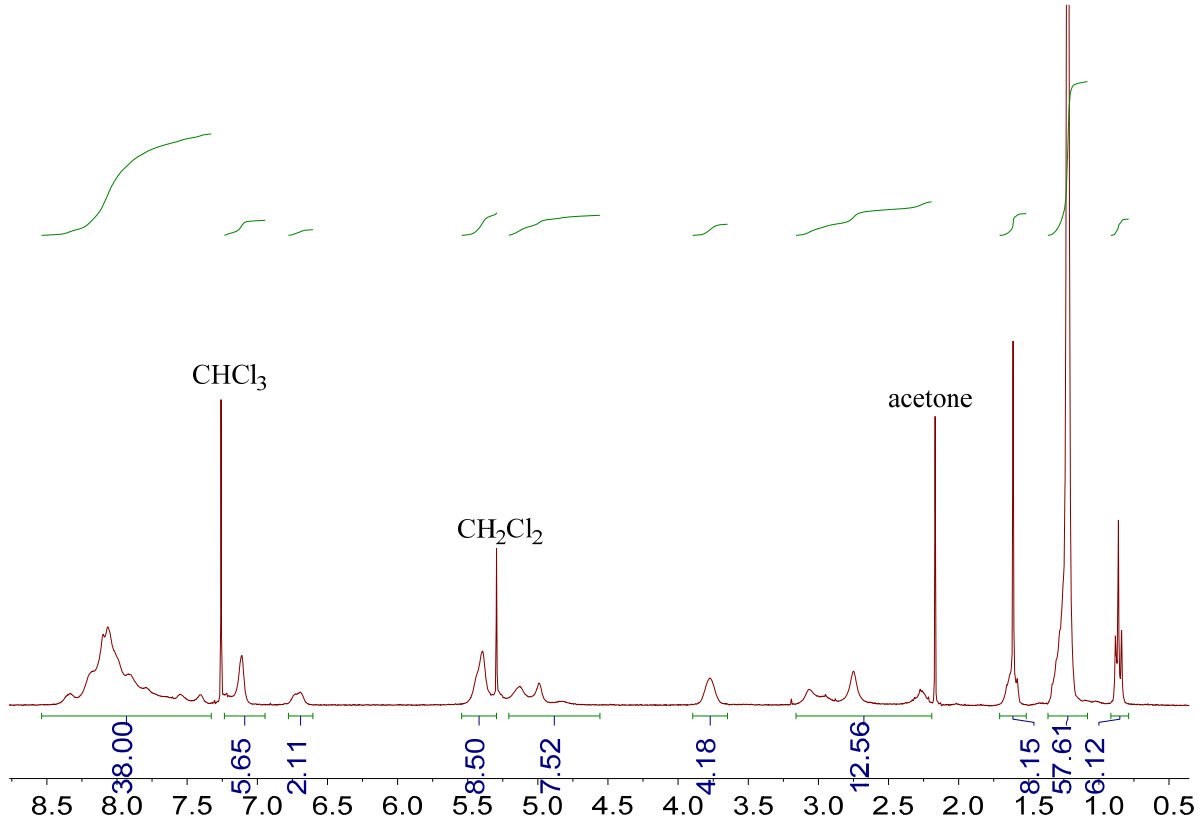


**Figure S51.** $^1$H NMR spectrum (300 MHz, $CDCl_3$, room temperature) of **8**.

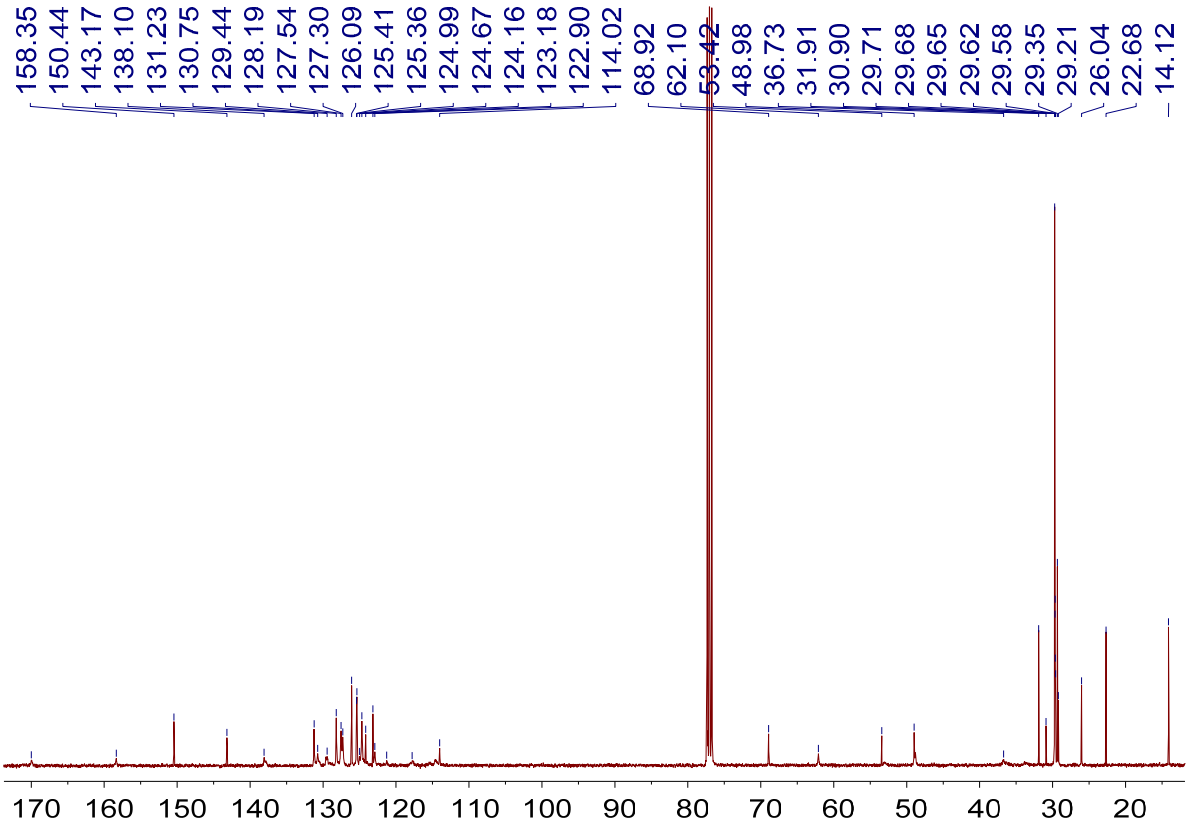


**Figure S52.** $^{13}C$ NMR spectrum (100 MHz, $CDCl_3$, room temperature) of **8**.

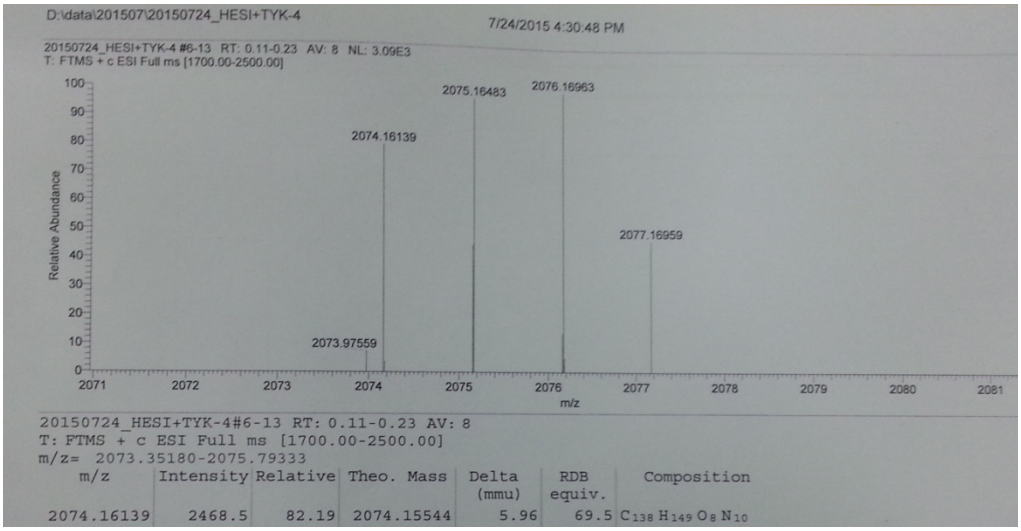


**Figure S53.** Electrospray ionization spectrum of **8**.

## *References:*


S1. Lim, WL.; Oo, CW.; Kobayashi, T. Photoluminescent enhancement of polyesters via photocrosslinking. *J. Appl. Polym. Sci.* **2015**, *132*, 41504.

S2. Wong, KMC.; Hung, LL.; Lam, WH.; Zhu, N.; Yam, VWW. A class of luminescent cyclometalated alkynylgold(III) complexes: synthesis, characterization, and electrochemical, photophysical, and computational studies of [Au(C ^ N ^ C)(C≡CR)] (C ^ N ^ C = $\kappa^3$C,N,C Bis-cyclometalated 2,6-Diphenylpyridyl). *J. Am. Chem. Soc.* **2007**, *129*, 4350–4365.

S3. Song, TK.; Teng, M.; Chandraratna, RA. **1998**, *WO9847854A1*.

S4. Tian, YK.; Shi, YG.; Yang, ZS.; Wang, F. Responsive supramolecular polymers based on the bis[alkynylplatinum(II)] terpyridine molecular tweezer/arene recognition motif. *Angew. Chem., Int. Ed.* **2014**, *53*, 6090–6094.

S5. Law, YC.; Kui, SCF.; Zhu. N.; Leung, KH.; Phillips, DL.; Che, CM. Ligand-to-ligand charge-transfer transitions of platinum(II) complexes with arylacetylide ligands with different chain lengths: spectroscopic characterization, effect of molecular conformations, and density functional theory calculations. *Chem. Eur. J.* **2010**, *16*, 6540–6554.

S6. Haedler AT, Misslitz H, Buehlmeyer C, Albuquerque RQ, Koehler A, Schmidt HW. Controlling the π-stacking behavior of pyrene derivatives: influence of H-bonding and steric effects in different states of aggregation. *ChemPhysChem.* **2013**, *14*, 1818–1829.

S7. Laederach, A.; Cradic, KW.; Brazin, KN.; Zamoon, J.; Fulton, DB.; Huang, X.; Andreotti, AH. Competing modes of self-association in the regulatory domains of Bruton's tyrosine kinase: Intramolecular contact versus asymmetric homodimerization. *Protein Science* **2002**, *11*, 36–57.

S8. Gaussian, 09.; Revision, A.; Frisch, MJ.; Trucks, GW.; Schlegel, HB.; Scuseria, GE.; Robb, MA.; Cheeseman, JR.; Scalmani, G.; Barone, V.; Mennucci, B.; Petersson, GA.; Nakatsuji, H.; Caricato, M.; Li, X.; Hratchian, HP.; Izmaylov, AF.; Bloino, J.; Zheng, G.; Sonnenberg, JL.; Hada, M.; Ehara, M.; Toyota, K.; Fukuda, R.; Hasegawa, J.; Ishida, M.; Nakajima, T.; Honda, Y.; Kitao, O.; Nakai, H.; Vreven, T.; Montgomery, Jr JA.; Peralta, JE.; Ogliaro, F.; Bearpark, M.; Heyd, JJ.; Brothers, E.; Kudin, KN.; Staroverov, VN.; Kobayashi, R.; Normand, J.; Raghavachari, K.; Rendell, A.; Burant, JC.; Iyengar, SS.; Tomasi, J.; Cossi, M.; Rega, N.; Millam, JM.; Klene, M.; Knox, JE.; Cross, JB.; Bakken, V.; Adamo, C.; Jaramillo, J.; Gomperts, R.; Stratmann, RE.; Yazyev, O.; Austin, AJ.; Cammi, R.; Pomelli, C.; Ochterski, JW.; Martin, RL.; Morokuma, K.; Zakrzewski, VG.; Voth, GA.; Salvador, P.; Dannenberg, JJ.; Dapprich, S.; Daniels, AD.; Farkas, O.; Foresman, JB.; Ortiz, JV.; Cioslowski, J.; Fox, DJ.; Gaussian, Inc., Wallingford CT, **2009**.

S9. Wu, RB.; Xie, HJ.; Cao, ZX.; Mo, YR. Combined quantum mechanics/molecular mechanics study on the reversible isomerization of glucose and fructose catalyzed by pyrococcus furiosus phosphoglucose isomerase. *J. Am. Chem. Soc.* **2008**, *130*, 7022–7031.

S10. Matsuda, SPT.; Wilson, WK.; Xiong, QB. Mechanistic insights into triterpene synthesis from quantum mechanical calculations. Detection of systematic errors in B3LYP cyclization energies. *Org. Biomol. Chem.* **2006**, *4*, 530–543.

S11. Figlus, M.; Tarruella, A. C.; Messer, A.; Sollisb, S. L.; Hartley, R. C. Low molecular weight MPEG-assisted organic synthesis. *Chem. Commun.,* **2010**, *46,* 4405–4407.